POLITECNICO DI MILANO

FACOLTÀ DI INGEGNERIA DEI SISTEMI
Corso di Laurea in Ingegneria Biomedica

Automatic localization of multilead intracerebral electrodes implanted for StereoElectroEncephaloGraphy

Relatore:
Ing. Elena DE MOMI

Correlatori:
Dott.ssa Chiara CABORNI
Dott. Francesco CARDINALE

Tesi di Laurea di:
Laura MILANI
Matricola 765645

Anno Accademico 2011-2012

Automatic localization of multilead intracerebral electrodes implanted for StereoElectroEncephaloGraphy

Laura Milani

April 22, 2013

Abstract

Epilepsy surgery is a surgical procedure aimed at the treatment of partial drug-resistant epilepsy. Its purpose is the resection of the epileptogenic zone, defined as the cortical region from which seizures originate and whose removal (or disconnection) is necessary for the complete suppression of the seizures. During the diagnostic phase, a multidisciplinar evaluation of the patient is necessary (epileptological anamnesis, video-EEG monitoring, structural and functional neuroimaging) for the definition of the epileptogenic zone. If these non invasive investigations fail to reach this objective, invasive intracranial recording is required.

StereoElectroEncephaloGraphy (SEEG) is an invasive diagnostic procedure which consists in the implantation of intracerebral multilead electrodes, according to a patient-tailored exploration strategy. During the video-EEG monitoring phase, depth electrodes allow recording the electrical activity directly from encephalic structures and, through electrical stimulation, the elaboration of a cortical functional map. A basic requirement of this phase is, therefore, the correlation between the recorded electrical signal and its anatomical source. The positions of electrodes contacts are checked performing post-implant computed tomography (CT) scans. CT produces three-dimensional images with relatively clear visibility of the electrodes contacts; however, due to the poor soft-tissue contrast, it does not allow a clear correlation of contacts position with respect to cortical structures.

The thesis project aims at developing a software tool able to reconstruct and localize, as accurately as possible, contacts of implanted electrodes with respect to the structural and functional brain anatomy. The developed module was embedded in 3D Slicer, an open-source multimodal environment for visualization and medical image computing. The required input dataset includes the preoperative magnetic resonance images (MRI), and a CT volume, acquired after the electrodes implantation. The method steps are:

- post-processing of the input MRI dataset using the open-source FreeSurfer software. The cortical volume, the segmented and parcellated brain volume based on the Desikan and Killiany atlas, the segmented cortical volume according to the Brodmann atlas and the 3D reconstruction of the pial surface are obtained. Likewise, the CT volume is processed allowing to obtain the skull-stripped postoperative volume;

- intensity-based analysis of the skull-stripped postoperative volume, from which the coordinates, in the CT imaging space, of the contacts centroids for all the electrodes implanted in a specific subject are extracted;

- selection by the user, through the module's graphical user interface, of the electrode he/she wants to reconstruct, from the dataset of implanted electrodes, and the polynomial regression curve order to model its trajectory;

- electrode reconstruction and visualization of its cylindrical-shaped contacts in the Slicer 3D view. Then, contacts are localized with respect

to the brain anatomy; in particular, for each contact whether it crosses gray matter (cortical contact), Desikan and Killiany atlas regions or Brodmann areas is determined. This information might be automatically stored in a file, the module output, with the possibility of creating a patients database.

A first analysis was performed in order to validate the algorithm's spatial accuracy. The positions of the reconstructed contacts centroids were compared with the surgeon identification of contacts centroids, through the positioning of fiducials in the center of the contacts artifact on the skull-stripped postoperative volume.

A second study was performed with the objective of verifying if a correlation exists between:

- the exploration pattern and the Desikan and Killiany atlas regions crossed by the contacts;
- the exploration pattern and the FreeSurfer available Brodmann areas that the electrodes go through;
- the Brodmann area at the entry point of the electrodes on the pial surface and the Desikan and Killiany segmented regions crossed during their trajectory.

Finally, a multivariate analysis (third analysis) was performed, using a mixed effect linear regression model, to determine if a correlation exists between the mean electrode curvature and several explanatory variables: the electrode's intracerebral length, the insertion angle and the Desikan and Killiany atlas regions.

Referring to the first analysis, the median value of the distances between the centroids reconstructed by the algorithm and the ones identify by the neurosurgeon resulted to be comparable to the image resolution. The algorithm spatial accuracy resulted greater with respect to a linear reconstruction of the electrode, given target point (electrode's tip) and entry point (on the cortical surface) direction. This difference further increases considering visually deviated electrodes.

The obtained results with the second analysis show that there is correlation, therefore the module resulted to be a useful tool for the localization of the sources of the electrical signals recorded during the post-SEEG monitoring phase.

Considering the multivariate analysis, the explanatory variables resulted to be linearly related to the electrode mean curvature are its intracerebral length and a Desikan and Killiany atlas region. Given that only one electrode in the modeled dataset was visually deviated, it will be necessary to perform the analysis on a dataset including a greater number of visually deviated electrodes.

Improvements can be directed to integrate into the module, embedded in 3D Slicer, the intensity-based analysis of the skull-stripped postoperative volume, to integrate other atlases into Slicer, based on the localization clinical needs, to

integrate the electrical signals associated to the respective contacts in the Slicer 3D view achieving a multimodal visualization environment. Even to define some parameters through which it would be possible to automatically classify an electrode as deviated or not, could alleviate the user to decide a regression's order for the curved model, since it would be directly modeled with the more appropriate curve.

The method presented in this work has been integrated in the 3D Slicer software present at the "C. Munari" Centre of Niguarda hospital. Then the clinical routine can be improved using the output of the module as important information for the diagnosis. Furthermore collecting all the SEEG exploration outputs can constitute a database on which performing interesting analysis in the future.

Key-words StereoElectroEncephaloGraphy, intracerebral electrodes, contacts segmentation, localization.

Sommario

La chirurgia dell'epilessia prevede un intervento chirurgico finalizzato alla cura di epilessie focali farmaco resistenti. Il suo obiettivo è la resezione della zona epilettologica, definita come la regione corticale da cui originano le crisi e che è necessario rimuovere (o disconnettere) per la completa abolizione delle crisi stesse. Durante la fase di diagnosi è necessaria una valutazione multidisciplinare del paziente (anamnesi epilettologica, monitoraggio video-EEG, imaging strutturale e funzionale) finalizzata principalmente alla definizione della zona epilettologica. Qualora le indagini non invasive non riescano a raggiungere questo scopo, è necessario ricorrere a tecniche invasive di registrazione intracranica.

La StereoElettroEncefaloGrafia (SEEG) è una procedura diagnostica mini-invasiva che prevede l'impianto di elettrodi intracerebrali multicontatto, secondo una strategia di esplorazione personalizzata per ogni singolo paziente. Durante la fase di monitoraggio video-EEG, gli elettrodi profondi impiantati consentono di registrare l'attività elettrica direttamente da qualsiasi struttura encefalica e, attraverso stimolazione, di elaborare una mappa delle funzioni corticali. Requisito fondamentale di questa fase è, quindi, la correlazione tra il segnale elettrico registrato e la sua sorgente anatomica. La posizione dei contatti degli elettrodi viene verificata dalle immagini di tomografia computerizzata (CT) acquisite a seguito dell'impianto. La CT produce immagini tridimensionali sulle quali i contatti degli elettrodi sono chiaramente visibili; tuttavia, a causa dello scarso contrasto dei tessuti molli, non permette di identificare una chiara correlazione tra la posizione dei contatti e le strutture corticali.

Il progetto di tesi ha come obiettivo la realizzazione di uno strumento software che sia in grado di ricostruire nel modo più accurato possibile i contatti degli elettrodi impiantati e localizzarli rispetto all'anatomia strutturale e funzionale del cervello. Il modulo è stato sviluppato e integrato in 3D Slicer, un ambiente open-source e multimodale per la visualizzazione e il trattamento delle immagini. Il dataset che richiede in ingresso è ottenuto a partire dalle immagini 3D preoperatorie di risonanza magnetica (MRI), e dal volume CT, acquisito in seguito all'impianto degli elettrodi. Le fasi previste dal metodo sviluppato sono:

- il post-processing del dataset di risonanza magnetica in ingresso, realizzato mediante il software open-source FreeSurfer e che consente di ottenere il volume corticale, il volume cerebrale segmentato e parcellizzato secondo l'atlante di Desikan e Killiany, il volume corticale segmentato con l'atlante PALS B12 Brodmann e la ricostruzione 3D della superficie corticale. Allo stesso modo, il volume CT è processato per ricavare il volume postoperatiorio a cui è stato sottratto il cranio;

- l'analisi del volume tomografico ottenuto dopo l'impianto: questa sfrutta l'intensità dell'immagine per ricavare le coordinate, nello spazio immagine, dei centroidi dei contatti per tutti gli elettrodi impiantati in uno specifico paziente;

- la selezione da parte dell'utilizzatore del modulo, per mezzo dell'interfaccia

grafica, dell'elettrodo che si intende ricostruire, dal dataset di elettrodi impiantati, e dell'ordine della curva polinomiale di regressione per modellare la traiettoria dell'elettrodo;

- la ricostruzione dell'elettrodo e la visualizzazione dei suoi contatti di forma cilindrica all'interno della vista 3D di Slicer. Il passo successivo è la localizzazione spaziale di ciascun contatto rispetto ad alcuni atlanti anatomici e funzionali; in particolare, per ciascuno di essi viene determinato se attraversa la materia grigia (contatto corticale) e quale/i regione/i dell'atlante di Desikan e Killiany attraversa. Per ciascun elettrodo vengono anche identificate le aree di Brodmann attraversate lungo tutto il suo percorso. Queste informazioni possono essere automaticamente memorizzate in un file, con la possibilità quindi di creare un database di pazienti.

Una prima analisi è stata condotta con lo scopo di validare l'accuratezza spaziale dell'algoritmo. La posizione dei centroidi dei contatti ricostruiti è stata confrontata con quella identificata dal chirurgo attraverso il posizionamento di fiduciali al centro dell'artefatto del contatto sul volume CT postoperatorio.

Un secondo studio è stato condotto al fine di verificare se esiste una correlazione tra:

- il pattern di esplorazione e le regioni dell'atlante di Desikan e Killiany attraversate dai contatti;
- il pattern di esplorazione e le aree di Brodmann che vengono attraversate dagli elettrodi;
- l'area di Brodmann attraversata da ciascun elettrodo all'ingresso della superficie piale e le regioni dell'atlante di Desikan e Killiany esplorate dai contatti durante la sua traiettoria.

Infine, è stata eseguita un'analisi multivariata, utilizzando un modello di regressione lineare a effetti misti, per determinare la presenza o meno di una correlazione tra la curvatura media dell'elettrodo e una serie di variabili esplicative: la lunghezza intracerebrale dell'elettrodo, il suo angolo di inserimento rispetto alla superficie del cranio e le regioni dell'atlante di Desikan e Killiany.

Facendo riferimento alla prima analisi, il valore mediano delle distanze tra i centroidi dei contatti ricostruiti dall'algoritmo e quelli identificati dal neurochirurgo è risultato essere comparabile con la risoluzione dell'immagine. L'accuratezza spaziale dell'algoritmo è risultata maggiore rispetto ad una ricostruzione lineare dell'elettrodo avente come direzione assegnata quella tra target point (punta dell'elettrodo) e entry point (ingresso dell'elettrodo nella corteccia). Questa differenza aumenta ulteriormente se si considerano elettrodi visivamente deviati.

I risultati ottenuti dalla seconda analisi mostrano che c'è correlazione e quindi il modulo sviluppato risulta essere uno strumento utile per la localizzazione delle sorgenti dei segnali elettrici registrati durante la fase di monitoraggio post-SEEG.

Per quanto riguarda l'analisi multivariata, le variabili esplicative che sono risultate essere linearmente associate con la curvatura media dell'elettrodo sono la lunghezza intracerebrale dell'elettrodo e una regione dell'atlante di Desikan e Killiany. Considerando che all'interno del dataset di elettrodi utilizzato per l'analisi, solo un elettrodo risultava visivamente deviato, sarà necessario eseguire nuovamente l'analisi includendo in esso un numero superiore di elettrodi visivamente deviati.

Gli sviluppi del lavoro qui descritto possono riguardare l'integrazione nel modulo dell'analisi intensity-based del volume CT postoperatorio, l'integrazione di altri atlanti, sulla base delle esigenze cliniche di localizzazione, e l'integrazione dei segnali elettrici registrati associati ai rispettivi contatti. Inoltre la definizione di parametri in virtù dei quali sia possibile classificare automaticamente un elettrodo come deviato o meno, solleverebbe l'utente dal dover scegliere l'ordine della curva per la regressione dell'elettrodo, perchè questo sarebbe direttamente approssimato con la curva più appropriata.

Il modulo presentato in questo lavoro è stato integrato in 3D Slicer ad uso dei clinici del centro di Chirurgia dell'epilessia dell'ospedale Niguarda. In questo modo, la normale pratica ospedaliera potrebbe beneficiare dei risultati ottenibili con questo strumento per ogni paziente esplorato, migliorando quindi l'accuratezza della diagnosi. Nel tempo la raccolta dei dati potrebbe anche costituire un database su cui eseguire interessanti analisi.

Parole chiave StereoElettroEncefaloGrafia, elettrodi intracerebrali, segmentazione dei contatti, localizzazione.

Contents

List of Figures

List of Tables

List of Algorithms

Chapter 1

Introduction

1.1 StereoElectroEncephaloGraphy

In drug-resistant partial epilepsy the pharmacological treatment is ineffective and the source of the seizures localized. The resection of the ictal onset zone is the most common and effective surgical option. The success rate of epilepsy surgery, leading to favorable outcomes regarding seizure control and avoidance of unacceptable neurological deficits, depends on the precise and accurate preoperative evaluation for defining the epileptogenic focus. The presurgical assessment of patients suffering from this pathology aims at localizing the spatial extent of the epileptogenic focus and relating it with highly eloquent ares of the cortex. Non-invasive presurgical investigations, such as accurate anamnesis, neurological examination, structural and functional neuroimaging and video-EEG monitoring, are performed. However, in about one-third of the subjects, non-invasive evaluations fail to identify the epileptogenic zone and/or the latter is adjacent to the eloquent cortex; in these cases, invasive intracranial monitoring may be indicated.

Different techniques of intracranial recording are currently used: grids and strips subdural electrodes, implanted beneath the dura on the cortical surface, and depth intracerebral electrodes. Subdural electrodes allow accurate mapping of large superficial cortical areas, but they provide limited coverage of deep-seated structures and of the cortex within sulci. Depth electrodes, instead, can sample mesial structures and the intrasulcal cortex, providing information from a limited volume of tissue. These last are stereotactically guided to subcortical structures during StereoElectroEncephaloGraphy (SEEG) procedures (Fig. 1.1 *left*). SEEG allows obtaining direct intralesional recordings and correlating interictal and ictal activity in three-dimensionally orientated areas of the brain (Fig. 1.1 *right*). This information is required in order to define the epileptogenic zone and create a cortical functional map. Accurate localization of the electrodes with respect to structural and functional brain anatomy is, therefore, an important part of surgical resection planning.

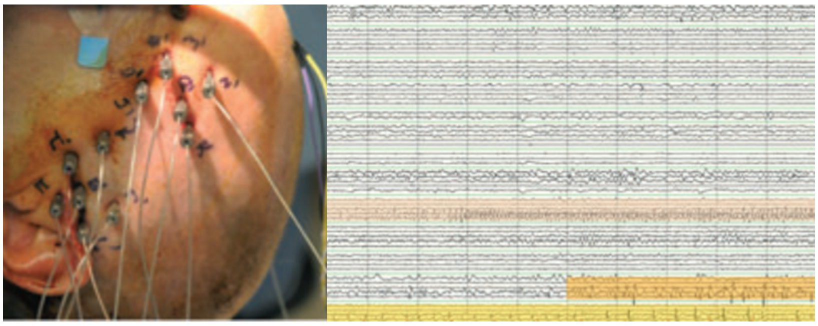

Figure 1.1: *Left:* intraoperative picture showing implanted electrodes during SEEG procedure. *Right:* SEEG recording.

1.2 Aim of the work: localization of contacts of implanted depth electrodes

During long term video-SEEG monitoring, in the postoperative phase of SEEG, it is possible to record spontaneous seizures, or to provoke them via low- and high-frequency stimulations. The localization of depth electrodes' contacts allows the clinician to identify the anatomical structure and crossed motor-sensory areas from which the electrical signal is generated and to map brain function. In fact, as the precise position of each electrode's contact is determined, a dynamic three-dimensional temporo-spatial picture of epileptic activity may be reconstructed (Fig. 1.2).

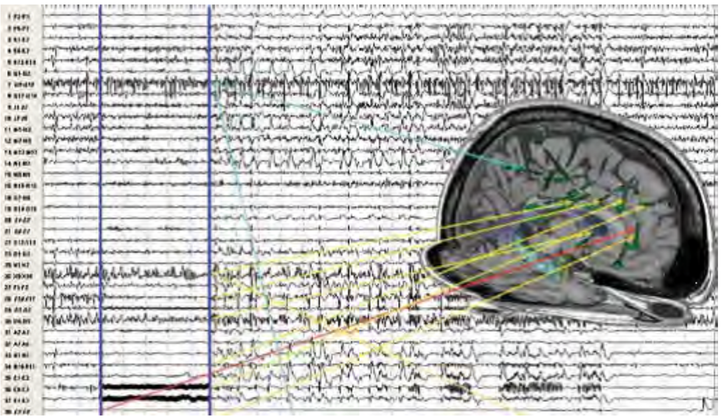

Figure 1.2: Example of correlation between the electrical signal recorded by electrodes' contacts and their anatomical position. Courtesy of [1].

The objective of this work is to automatically localize the contacts of each implanted depth electrode in order to correlate the signal recorded by each contact of the trajectory with its anatomical position and to develop a software tool for postoperative SEEG implantation analysis and assessment.

This work has been realized at Nearlab, Politecnico di Milano, through the collaboration with the team working at "Claudio Munari" Center for Epilepsy and Parkinson Surgery, Niguarda Ca' Granda Hospital, Milan, Italy, in particular the M.D. Francesco Cardinale, who made available data and clinical competences, and Gabriele Arnulfo, PhD at Università degli Studi di Genova, who provided the intensity-based image analysis code used as starting point of the work.

1.3 Outline of the thesis

The thesis is organized as follows:

- Chapter 2 describes the SEEG procedure with a summary of information from clinical centers performing the SEEG methodology and summarizes the state of the art in the electrodes contacts localization for deep brain stimulation context and for subdural grids.
- Chapter 3 presents the materials and the developed methods used for the reconstruction and the localization of multilead intracerebral electrodes implanted in SEEG procedures, together with the experimental protocol and the performed analysis on 29 patients who underwent SEEG electrodes implant.
- Chapter 4 reports the experimental results of the performed analysis.
- Chapter 5 concludes the thesis and presents possible future developments for the presented work.

Chapter 2

State of the art

2.1 StereoElectroEncephaloGraphy

StereoElectroEncephaloGraphy (SEEG) is a diagnostic stereotactic procedure aimed at implanting recording multilead depth electrodes directly within brain structures, with a patient-tailored exploration strategy on the basis of noninvasive studies [1]. It may be used in patients with epilepsy not responding to medical treatment, and who are potential candidates to receive brain surgery in order to minimize/dissolve seizures.

Intracerebral electrodes are placed within the desired brain areas to record spontaneous seizures or to provoke them via low- and high-frequency stimulations, thus contributing to define with accuracy the epileptogenic zone, i.e. the site of the beginning and of primary organization of the epileptic discharge [12].

This technique was developed and introduced in the diagnostic iter of epileptic patients by Talairach and Bancaud at the S. Anne Hospital, Paris, France, in the second half of the 20th century [13]. Nowadays the basic concepts of this methodology are still valid, but modern technological tools facilitate the workflow, as the integration of advanced multimodal imaging, obtained in frameless conditions, and robotic surgical implantation [14].

The main steps of the SEEG procedure are:

- medical imaging acquisition (MRI, ...), post-processing and electrodes' trajectories planning;
- implantation of the electrodes and postoperative imaging (CT) to check electrodes placement;
- video-SEEG monitoring, electrodes removal, data analysis and surgical resection planning.

Tables 2.1 and 2.2 summarize information collected from worldwide clinical centers performing the SEEG methodology, about patients clinical characteristics, pre-operative imaging and topographic brain regions explored [15, 16, 17, 18, 14, 19, 20, 21]. The number of SEEG procedures per year ranges between 15 and 30, with a minimum of 1 and a maximum of 50 and with a mean number of electrodes implanted per patient approximately equal to 11/12. Subjects who underwent SEEG electrodes implantation are of young age, with the onset of the seizures approximately at ten years old and a duration of the epilepsy of about fifteen years. The preoperative images most widely used are the angiography and the MRI.

2.2 Electrode contacts localization methods

The localization of electrodes' contacts is an issue adressed both in deep brain stimulation (DBS) and epilepsy surgery context.

In DBS context, in order to analyze differential effects of stimulation on specific symptoms and on the evocation of adverse events, program stimulation parameters and correlate electrode placement with intraoperative neurophysiological mapping, precise electrodes contacts localization is needed [22].

In the field of epilepsy surgery, for a correct interpretation of the electroencephalographic and mapping data and for the planning of the subsequent surgical procedure, the information about the exact position of the implanted electrodes with respect to relevant brain structures is essential [7]. No studies concerning this problem have been found in literature in the SEEG context but only regarding subdural grids electrodes.

2.2.1 Deep brain stimulation electrodes localization

DBS electrodes are composed of four cylindrical-shaped stimulating contacts. They are located at the tip of the electrode. In all the studies reported hereafter the same electrode's model is used, Activa 3389 (Medtronic, Minneapolis, Minn., USA) (Fig. 2.1). Each contact is 1.5 mm high and 1.27 mm wide.

Figure 2.1: Activa 3389 DBS electrode.

Several authors described methods for DBS electrode localization based on magnetic resonance imaging (MRI) [2, 3, 23, 22, 4, 5]. The approach proposed

	Mean patients (per year) (F/M)	Age at SEEG (years) (±SD)	Sz onset (years) (±SD)	Ep duration (years) (±SD)	Electrodes number (Mean per patient)	U/B	Pre-operative images
A	50 (46/54)	32	10	15	1310 (13)	60/40	–
B	23,3 (34/36)	25,2 (±9,2)	9,5 (±7,2)	15,7 (±7,6)	714 (10,2)	60/10	Angiography 2D Ventriculography
C	3,7 (14/7)	20,3 (±14,2)	10,7 (±13,9)	–	107 (5,1)	–	MRI
D	20 (55/45)	35	–	–	1118 (11)	–	Angiography 2D MRI
E	31,3 (198/284)	25,99 (±11,8)	8,07 (±6,89)	17,94 (±10,51)	6496 (12,99)	425/75	Angiography 3D MRI (T1-weighted)
F	15,8 (242/249)	30,4 (±12,4)	10,9 (±10,4)	19,7 (±12,4)	2943 (6)	–	MRI Double-dose Gd MRI
G	15 (7/8)	6.5	–	–	172 (11,5)	13/2	–
H	0,9 (17/11)	16,5	2,75	12	257 (8)	13/15	Angiography 2D MRI

A: Epilepsy Center, Neurological Institute, Cleveland Clinic, Cleveland, Ohio, USA
B: Grenoble Epilepsy Surgery Center, Grenoble, France
C: Epilepsy Unit in Cerrahpasa Medical Faculty, Istanbul, Turkey
D: Department of Functional Neurosurgery, Lyon, France
E: Claudio Munari Center for Epilepsy Surgery, Milan, Italy
F: Montreal Neurological Institute and Hospital, Montreal, Quebec, Canada
G: Fondation Rothschild, Paris, France
H: Sainte-Anne Hospital, Paris, France

Table 2.1: Clinical characteristics of the patients population and pre-operative imaging. F: females; M: males; SD: standard deviation; Sz: seizure; Ep: epilepsy; U: unilateral investigations; B: bilateral investigations.

	Frontal lobe (no. of procedures)	Occipital lobe (no. of procedures)	Parietal lobe (no. of procedures)	Temporal lobe (no. of procedures)	Others (no. of procedures)
A°					Multilobar 100
$B^{\sim}$	53	11	52	64	–
C°	2	0	0	3	Multilobar 16
D	–	–	–	–	–
$E^{\wedge}$	Frontal 32 Fronto-central 104 Fronto-insulo-perisylvian 35 Fronto-temporal 65	Occipital 28 Postero-central 33	–	Temporal 14 Temporo-insulo-perisylvian 46 Temporo-posterior 107	Diffused 29 Perilesional 7
F°	90	15	10	329	Central 6 Multilobar 41
G^{-}	61	8	27	55	Opercula 21
H	–	–	–	–	–

A: Epilepsy Center, Neurological Institute, Cleveland Clinic, Cleveland, Ohio, USA
B: Grenoble Epilepsy Surgery Center, Grenoble, France
C: Epilepsy Unit in Cerrahpasa Medical Faculty, Istanbul, Turkey
D: Department of Functional Neurosurgery, Lyon, France
E: Claudio Munari Center for Epilepsy Surgery, Milan, Italy
F: Montreal Neurological Institute and Hospital, Montreal, Quebec, Canada
G: Fondation Rothschild, Paris, France
H: Sainte-Anne Hospital, Paris, France

Table 2.2: Distribution of implanted electrodes. $^{\circ}$: region exploration with all the electrodes; $^{\sim}$: region exploration with at least one electrode; $^{\wedge}$: region exploration by most of the electrodes; $^{-}$: no. of electrodes.

by [2] uses as input a postoperative (3D T1-weighted magnetization-prepared rapid acquisition gradient echo (MPRAGE)) imaging sequence. First, the distal artifact is manually identified following the main axis of the electrode; from a previous work of the same authors that analyzed the real electrode (Activa 3389; Medtronic) position within the MRI (3D T1-weighted MPRAGE sequence) artifact in an in-vivo and an in-vitro study, it was found that the distal artifact and the center of the distal contact (C0) are separated by 2.15 mm. Next, the angle of the electrode with the vertical is measured on sagittal and coronal slices (Fig. 2.2). Then, knowing the relationship between the electrode MRI artifact and related contact and the electrode physical specifications, it is possible to deduce the coordinates of the centers of the four contacts (C0,C1,C2,C3).

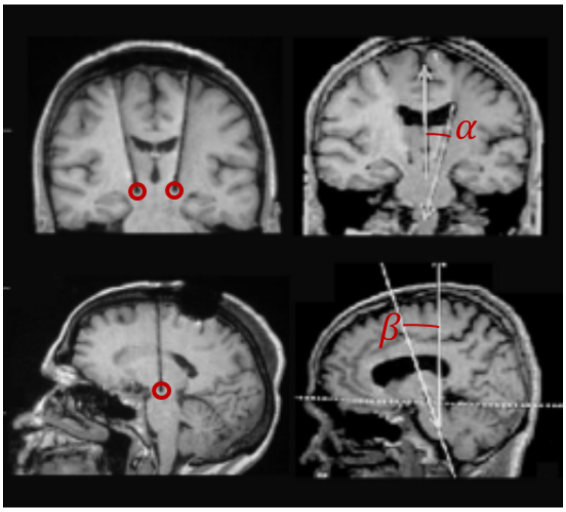

Figure 2.2: Magnetic resonance images demonstrating the procedure to localize the implanted electrodes. *Left:* identification of the limit of the distal artifact on coronal *(upper)* and sagittal *(lower)* slices, following the main axis of the electrode. *Right:* measurement of the angles (α, β) between the electrode and the vertical plane in coronal *(upper)* and sagittal *(lower)* slices. Adapted from [2].

The accuracy of this method can be affected by:

1. imprecision in identifying the distal limit of the C0 artifact resulting from the voxel size of the magnetic resonance image;
2. imprecise identification of the angles of the electrode on coronal and sagittal plane, leading to increasing errors from C0 to C3. An overestimation of 5° in these two angles would induce on C3 an anterior and lateral shift of approximately 0.6 mm;

3. errors resulting from image distortion on MRI. This kind of error has already been evaluated and was found inferior to 1 mm in each axis.

Two similar methods are presented in [3, 23]. [3] uses a MRI T1-weighted volumetric sequence on axial and coronal planes, while the input in [23] is a 3D MRI volumetric gradient-echo image set followed by an axial T2-weighted fast-spin echo pulse sequence. Using Stealth FrameLink 2.0 software (Medtronic, Inc., Minneapolis, MN), MR images are reformatted to be parallel to the anterior commissure (AC)-posterior commissure (PC) plane and subsequently are superimposed onto the Schaltenbrand and Wharen atlas with a rigid registration. The next step is the manual identification of the coordinates relative to the electrode's tip and its entry point into the brain respectively, thus linearly reconstructing the entire trajectory. The manually selected center of the observed MRI round artifact on three orthogonal planes is considered to represent the true tip position (Fig. 2.3). Contacts coordinates are then calculated along the reconstructed trajectory taking into account the geometry of the electrode.

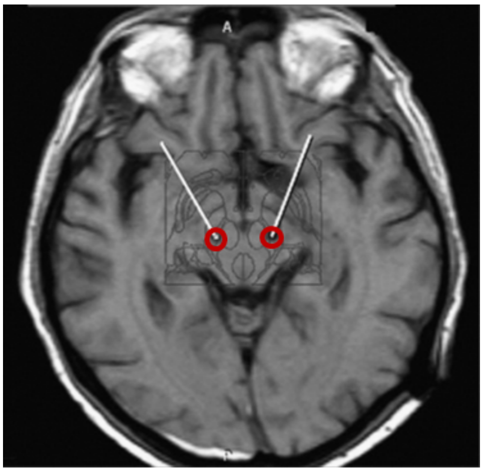

Figure 2.3: Manually identification of electrodes' tips. Adapted from [3].

A similar approach to the one described above is presented in [22]. The position of the electrodes is assessed postoperatively using a high-resolution T2-weighted fast-spin echo sequence. First, considering the presence of an electrode image artifact that makes electrodes larger than their actual size, its center is used to determine the coordinates of the electrode's tip. Then the angles of implantation are directly manually measured on the images and the electrode's trajectory is linearly reconstructed in all three planes. Finally, electrode's contacts along the reconstructed trajectory are plotted according to the known dimensions of the electrode. The verification of the accuracy of this method is given by postmortem histological analysis. Data from several postmortem cases revealed that there is a correspondence within 1 mm between the

MRI-determined location and the actual electrode's position reconstructed from histological sections.

In [4] a different procedure is proposed. A MRI MPRAGE is postoperatively acquired. Localization of the electrode and four contacts is performed by isosurfacing the electrode's artifact in the MR images. At successively lower isovalues, the isosurface converged onto the four electrode's contacts, as shown in Fig. 2.4. No studies regarding the localization accuracy of this method are presented.

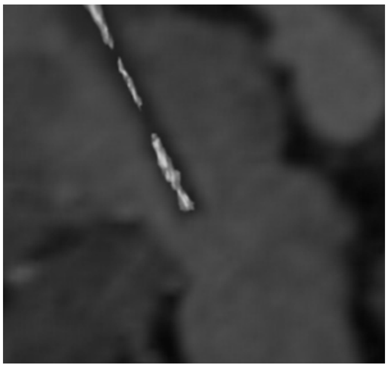

Figure 2.4: Intensity values around the electrode's halo are isosurfaced with progressively lower values until the surface converged onto the electrode's contacts. Courtesy of [4].

Pinto et al. [5] compared two image acquisition modalities to determine the implanted electrode placement into the subthalamic nucleus, used in several centers providing DBS for Parkinson's disease patients. The first input is a ventriculography (Vg) acquired intraoperatively. Vg provides an accurate visualization of the AC and PC, as well as the delineation of the third ventricle (V3) without magnetic image distortion. However, mostly because of its invasiveness, Vg is performed at only few centers. For each electrode's contact, the three coordinates (the mediolateral x coordinate, the anteroposterior y coordinate and the dorsoventral z coordinate) are manually identified considering the middle of the contact image in three dimensions (Fig. 2.5). The second input considered to visualize electrodes' trajectories and contacts is a postoperative MRI spin-echo T1-weighted (SET1) sequence in the sagittal and coronal planes. The same reference axes as those used for Vg are considered. The middle of the hypointense signal is considered as the center of the contacts and manually chosen by visual inspection (Fig. 2.6, Fig. 2.7). Giving Vg and SET1 measurements, significant differences were found for the x coordinate (both left and right side) and for the y coordinate, the right side: for the x coordinate and the y coordinate of the contacts a trend toward a right and an anterior translation, respectively, seemed probable when measured using SET1 images. No statistical differences were found for the z coordinate (left and right side) and for the y coordinate, the left side.

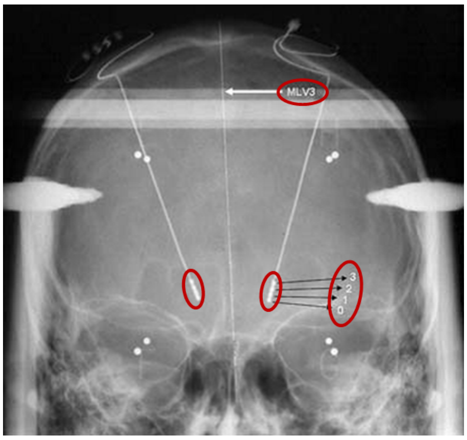

Figure 2.5: Intraoperative Vg for implanted electrodes localization. MLV3, reference axis; 0, 1, 2, 3, the four contacts of the implanted electrodes. Adapted from [5].

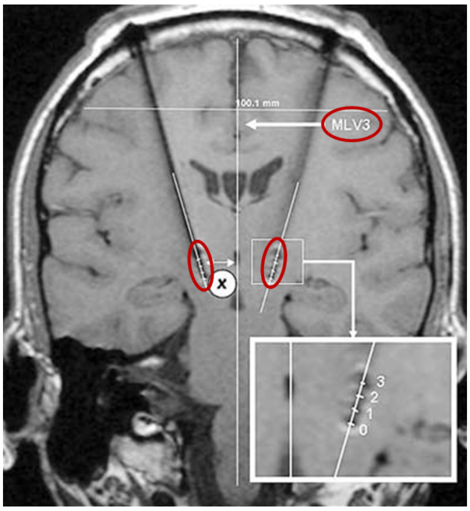

Figure 2.6: Postoperative frontal spin-echo T1-wighted image for the determination of the x coordinate (mediolateral) of the electrodes' contacts. MLV3, reference axis; 0, 1, 2, 3, the four contacts of the implanted electrodes. Adapted from [5].

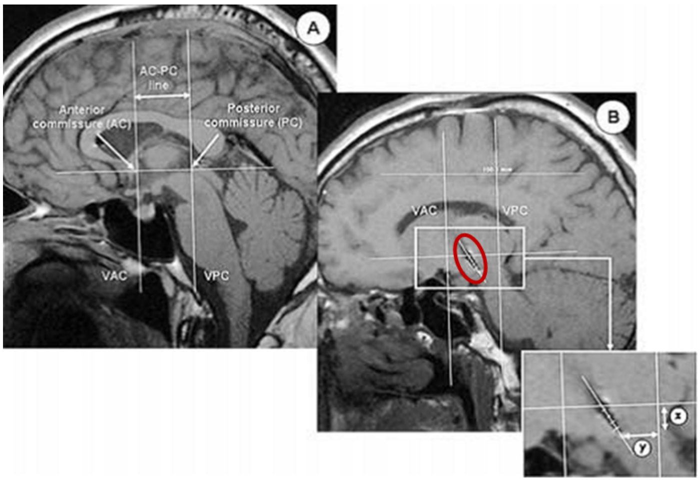

Figure 2.7: (A): postoperative sagittal SET1 MRI slice for measurement of the AC-PC line, reference axis for z coordinate determination. (B): determination of the anteroposterior y and dorsolateral z coordinates of the electrode's contacts. VAC, vertical line (orthogonal to the AC-PC line) passing through the AC; VPC, vertical line (orthogonal to the AC-PC line) passing through the PC, reference axis for y coordinate determination. Adapted from [5].

Differently from the approaches described so far, in [6] the contacts' position analysis of DBS electrodes is carried out using postoperative CT images. CT acquisitions show the presence of a white artifact corresponding to the electrode and a lateral black artifact around a part of the electrode due to the difference in density between the contacts and the surrounding tissue. Similar to what is presented in [2], this study undertakes an electrode's artifact analysis to obtain information on the artifact's dimensions and related electrode's contact positions. The proposed analysis identifies by visual inspection the distal boundary of the lateral black artifact corresponding to the end of the distal contact and the proximal boundary of the lateral black artifact corresponding to the beginning of the proximal contact. As there might be a discrepancy between the extremities of the distal and proximal contacts and their respective black artifact boundaries, the authors recommend using the midpoint between the distal and proximal black artifact boundaries as a reference to calculate the location of the four contacts, according to the electrode's geometry (Fig. 2.8). No studies regarding the localization accuracy of this method are presented.

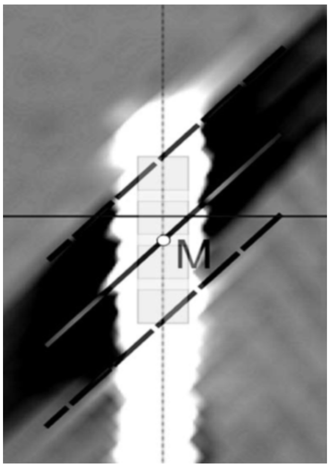

Figure 2.8: Identification of the distal and proximal black artifact boundaries and determination of the four contacts' location relatively to the point M placed in the middle of the distance between the two boundaries. Courtesy of [6].

As said, all the presented methods are based on the manual identification on the postoperative images of the information necessary for the reconstruction of the electrode trajectory or, directly, of the electrode's contacts. A similar approach, applied to the SEEG context, is extremely time-consuming considering that a mean of 13 electrodes per patient is usually implanted in SEEG procedures. Furthermore, the number of contacts in depth electrodes is greater than that of the DBS electrodes. Moreover, a linear reconstruction of the electrode's trajectory does not take into account of a possible electrode deformation.

2.2.2 Subdural grid electrodes localization

Subdural grid electrodes consist of a matrix, of variable size, of contacts embedded in a silastic sheet. Contacts have a exposed diameter of 2.3 mm and a inter-contact spacing of 1 cm center-to-center (Ad-Tech Medical, Racine, WI, USA) (Fig. 2.9). For grid placement, craniotomy with opening the dura is performed over the cortex area to be recorded.

The position of subdural electrodes after implantation is estimated by a number of methods, including 3D MRI [7, 24, 8], its superimposition with postoperative CT [9, 25, 26, 10, 27, 28] and coregistation between digital photographs, MRI and radiographs [11].

In [7] 3D MRI datasets are acquired using a MPRAGE sequence before and after the implantation of the subdural electrodes. Image data processing steps, as summarized in Fig. *2.10,* are:

- coregistration of the post-implantation image to the pre-implantation image using a rigid transformation (1);

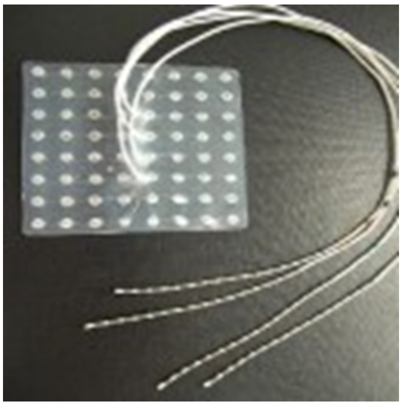

Figure 2.9: Subdural grid electrodes consist of 64 contacts arranged in a 8x8 matrix.

- normalization of the pre and coregistered post-implantation image to the standard brain of the Montreal Neurologic Institute (http://www.mni.mcgill.ca/) (2a and 2b);
- brain extraction in the pre-implantation image [29] (3a);
- brain extraction in the post-implantation image by using the skull-stripped pre-implantation image as a mask (3b).

Because of their artifacts, the locations of electrodes' contacts are directly visible in planar MR sections.

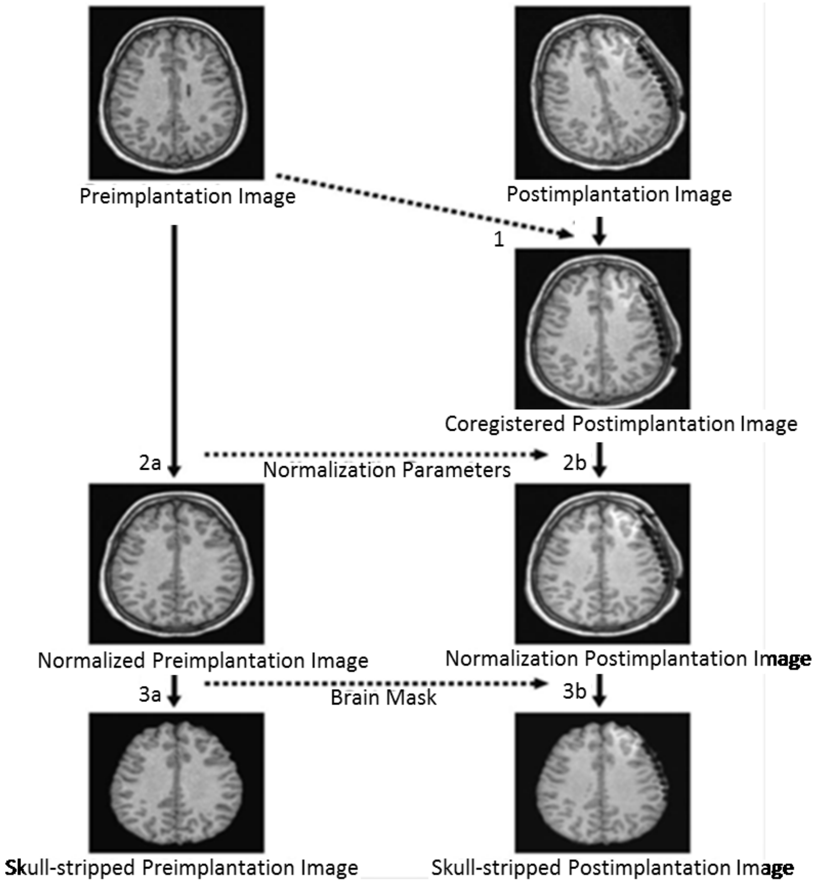

Figure 2.10: Steps of the image data processing. Courtesy of [7].

T1-weighted MR images acquired prior to and within 24 hours after electrodes implantation are the inputs in the subdural grids localization procedure presented in [8] (Fig. 2.11 A, B). First the pial surface and the smoothed pial surface are reconstructed (Fig. 2.11 C), based on the pre-implant MR image, and the two collected image datasets are coregistered (Fig. 2.11 D). Next, for each grid electrode, three contacts must be manually localized on the coregistered post-implant image. The remaining grid contacts are interpolated on the plane determined by the previously manually localized contacts using the known inter-contact distance. To project this set of planar coordinates (G) onto the smoothed pial surface with respect to some center of projection (c), a patch of the cortical surface (B) is isolated (Fig. 2.11 E). The next step is the research of the center of projection: the patch's center of curvature, defined as the point equidistant to all of the vertices of B is considered. Starting from an initial estimated of the point c, the search space is constrained to points along the c-m axis, where m is the center of mass of G. At each iteration the point c is shifted back and forth along the c-m axis and lines connecting the current c with each point in G are drawn in order to find their intersection with B (I) (Fig. 2.11 E). The set of inter-electrode distances {d} between pairs of neighboring points in I is also computed. The iterative optimization finishes when the accuracy level (in terms of distance between {d} and the known inter-contacts distance) set by the user is reached; the contacts localization spacial accuracy of this algorithm is validated using intraoperative photographs and it's calculated to be 0.96±0.81 mm.

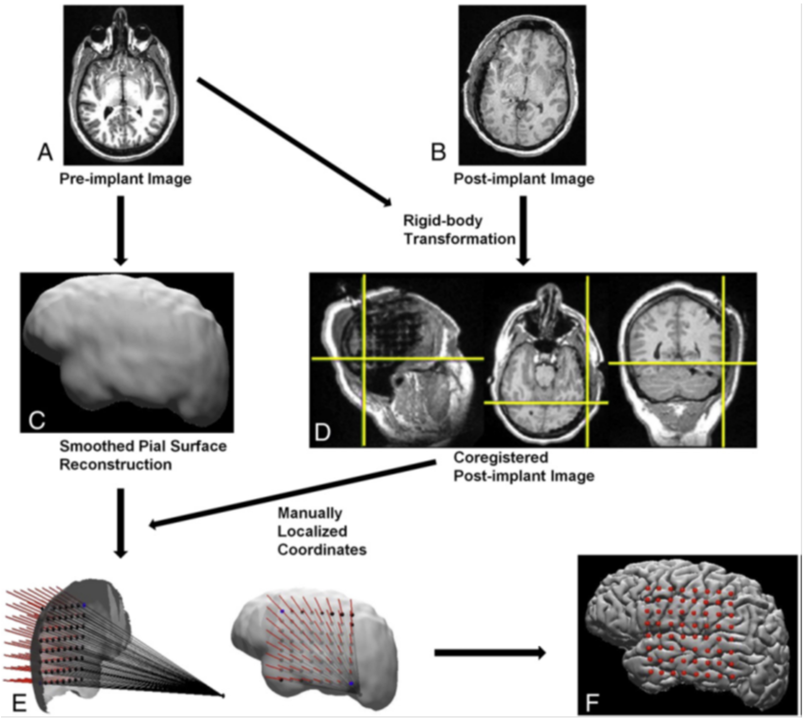

Figure 2.11: Procedure for localization of grid electrodes from pre- and post-implant MR images. Courtesy of [8].

The procedure proposed in [9] uses as inputs an high-resolution T1-weighted MRI, acquired preoperatively, and a postoperative CT, which is automatically registered to the MRI image using a mutual information-based transform algorithm. The maximum intensity projection of the CT volume in the plane approximately perpendicular to the long axis of the contacts arrays is computed (Fig. 2.12 A). After locating each contact in the 2D image, the final contact's coordinates are obtained by traversing slices in the 3rd dimension and selecting the approximate center of the hyper intensity created by each contact. This procedure yielded an initial estimate of a subdural electrode's coordinate on the cortical surface (left panel of Fig. 2.12 B). After the 3D rendering of the cortical surface and the smoothed pial surface using the MRI, the procedure accounts for the brain deformation caused by the surgical implant pulling the initial coordinates estimates to the smoothed pial surface via an energy-minimization algorithm. All contacts have to lie on the smoothed pial surface, while minimizing the displacement between original and current contact location as well as the deformation in the spatial configuration of the contacts. After the contacts are pulled to the smoothed pial surface, they are projected to the closest vertex (in Euclidean distance) on the pial surface (right panel of Fig. 2.12 B). Validation of the localization procedure is carried out through computation of the Euclidean distance between the location estimated and that determined by visual inspection of intraoperative photographs and is within 3 mm on average on five electrodes.

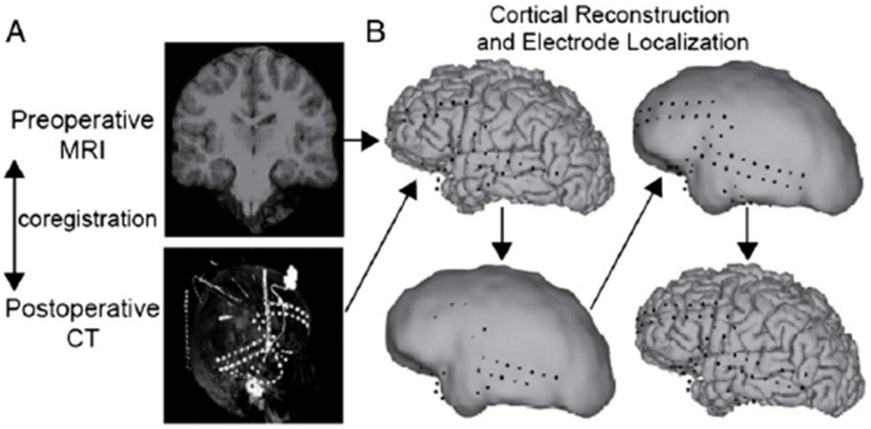

Figure 2.12: Outline of electrode localization procedure. (A): The preoperative MRI is coregistered with the postoperative CT volume. The lower panel shows the maximal-intensity projection of the CT volume in the sagittal dimension, which shows all the contacts in a sagittal plane. (B): Due to the parenchymal shift from the implant procedure, some contacts initially appear buried in the gray matter (left panel). To correct for this, each contact coordinate is projected first to the smoothed pial surface and subsequently back to the pial surface (right panel). Courtesy of [9].

The preoperative volumetric MRI (with T1-weighted sequences) and the postoperative CT scan are the inputs in [25]. The MRI data are segmented to enable the extraction of the contours of the brain surface; afterward, the skull as visualized in the CT and as extracted from segmented MRI data is used as template to fuse MRI and CT. The electrodes' contacts are detected considering three parameters: the voxel mask size, the brightness and contrast thresholds and the minimum and maximum distance between selected voxels to discriminate each contact within a grid and each contact within different grids respectively. To verify the accuracy of the contacts detection and localization method, their position is compared with the position of the same contacts that are visible in digital photographs taken intraoperatively. The quantitative evaluation of their mismatch yields a value of 2±0.12 mm.

The procedure of localization of subdural electrodes presented in [26] consists in the registration of the preoperative MR and postoperative CT data sets by interactive manual transformation of the CT study over the MR image to produce a combined dataset showing electrodes, which are displayed three-dimensionally.

The methods developed in [10, 27] performed registration between pre and post-implantation image datasets, segmentation and 3D rendering. In [10] the first step is automatically realized using the normalized mutual information algorithm; then the brain is segmented in the MRI dataset, as well as the subdural electrodes of the CT scan by a threshold algorithm. Afterward, the segmented data are visualized in three dimensions. In [27] four anatomical landmarks are used for matching the internal coordinate systems of MRI and CT. The coordinates of subdural electrodes are digitized from CT images contact by contact and visualized on the cortical surface segmented from MRI.

After the registration between MRI and CT scans, in [28], approximate locations of electrode's contacts are identified manually on the CT by selecting high intensity clusters. Then these clusters are automatically masked by thresholding and the center of mass of each cluster is assumed to be the position of a contact (Fig. 2.13 A,B,C). Each contact is then projected to the cortical surface of the coregistered MRI scan in the direction of the local norm vector of the electrode grid (Fig. 2.13 D,E,F). To estimate the accuracy of the projection method, the projected contacts are visualized on a 3D rendering of the cortical surface (Fig. 2.13 G) and compared to photos taken during implantation procedure. The median distance between the projected contacts and the ones on the photo is 2.6 mm.

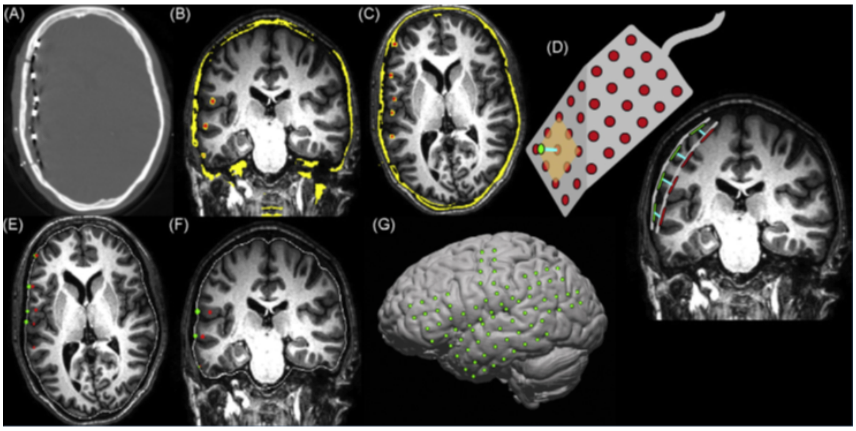

Figure 2.13: Schematic representation of the projection method. (A): Slice of the CT scan; (B and C): thresholded CT (yellow), with detected contacts (red), overlaid on a MRI, with contacts shifted beneath the pre-implantation surface; (D, E and F): contacts located under the cortical surface (red) are projected to the cortical surface (green) in the direction of the normal vector of the grid (blue lines in D); (G): rendering of the cortex with projected contacts. Courtesy of [10].

Unlike the procedures described so far, the one presented in [11] is based on multiple image sets, specifically: high-resolution T1-weighted MRI scans, skull film radiographs and digital photographs taken during electrodes surgical implantation. The steps of the algorithm are:

1. registration of surgery photographs, one showing the exposed brain (anatomical photograph, Fig. 2.14 B) and one showing the contacts grid on top of the brain (grid photograph, Fig. 2.14 A);

2. registration between photograph and MRI through a manually annotation of the location of visible contacts from the photograph on the MRI surface rendering of the patient brain (Fig. 2.14 C);

3. registration between MRI and radiograph. Contacts' positions, as shown in the radiograph (Fig. 2.14 D, dark dots), and the ones obtained in the previous step (Fig. 2.14 D, green circles) are used as control pairs to generate the MRI-radiograph transformation. This last is used to compute the location of the X-ray source and trace the path of the X-rays that generated the image of each contact. Surface electrodes are the intersection of these rays with the cortical surface (Fig. 2.14 E,F).

Electrodes' positions found using this method has a mean discrepancy of 1.5±0.5 mm when compared to the photograph-derived coordinates.

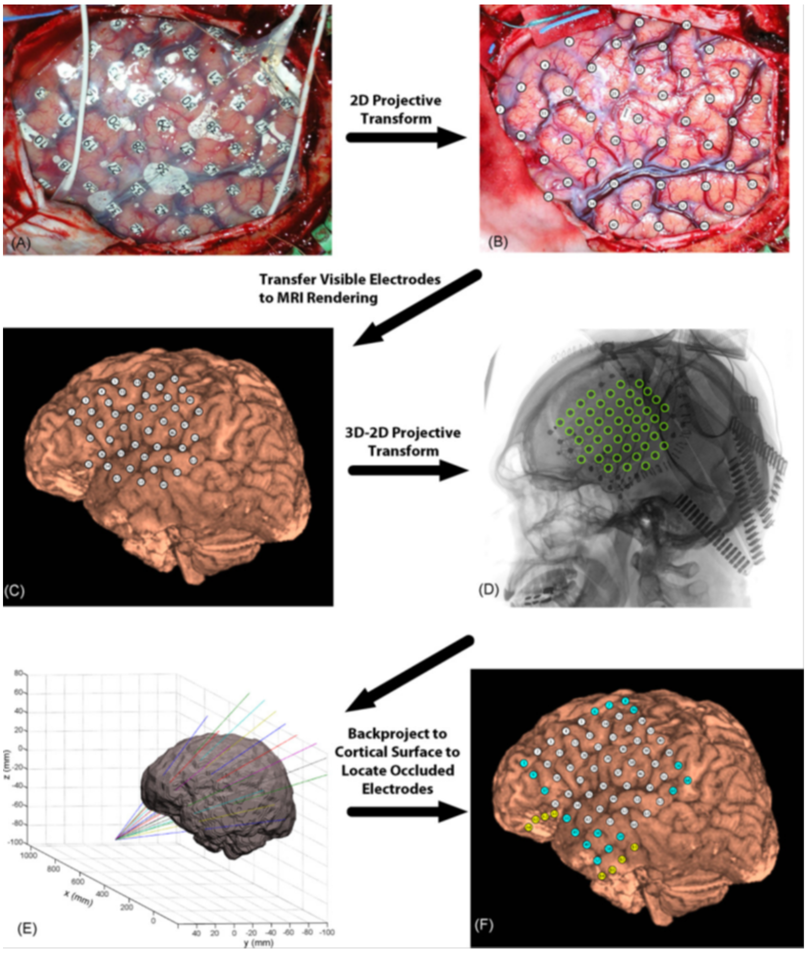

Figure 2.14: Procedure for registration of electrodes from photographs, MRI, and X-ray. Courtesy of [11].

As said, the methods described in [7, 24, 8] use MRI for post-implantation imaging. Despite it can visualize brain anatomy with high fidelity, magnetic susceptibility artifacts caused by the electrodes are larger than those on CT scans: from MRI scans published in the literature, contacts with spacing tighter than 1 cm are indistinguishable [11]. Therefore, the electrode artifact can obscure both the contacts positions and the morphology of the underlying cortical surface. The procedures presented in [9, 28] face with the brain shift introduced by the implantation of subdural electrodes. It may cause a significant mismatch between the post-implant CT and the MRI obtained preoperatively, potentially causing localizations errors. The brain shift does not affect the SEEG procedures, which are mini-invasive, not requiring craniotomy. For the same reason, intraoperative photographs, as used in [11], are not applicable. The reported mean errors in the positions of localized contacts range from a minimum of 0.96 mm to a maximum of 3.00 mm.

Chapter 3

Materials and Methods

In this chapter the developed methods for the electrode reconstruction and contacts localization are presented. Then, the performed analysis are described.

3.1 Intracerebral electrodes

The electrodes implanted during SEEG procedures are semi-rigid multilead depth electrodes with 0.8 mm external diameter (Fig. 3.1). Every contact is 2 mm long, with 1.5 mm inter-leads gap. These electrodes are available with 5, 8, 10, 12, 15, 18 contacts, without or with the presence of groups of leads (3 groups with 5, 6 contacts each).

Figure 3.1: Multilead intracerebral electrode manufactured by Dixi Medical (Microdeep Intracerebral Electrodes®, Besançon, France).

3.2 Virtual environment

The work was performed using 3D Slicer, an open-source software for the analysis and visualization of medical images. It's an extensible and scriptable development platform. The electrode analysis method was implemented using VTK (Kitware, Clifton Park, NY, US), CTK and Qt (Qt software, Oslo, Norway) libraries. A module written in Python language was developed and integrated in 3D Slicer. The VTK scientific library was used for the processing and visualization of data; the CTK and Qt libraries were used for the interface description.

3.3 Input data

Different types of data constitute the input to the module. They are:

- preoperative T1-weighted MR images, acquired, using 1.5T (Intera Achieva, Philips Medical System, The Netherlands), on the sagittal plane (0.90 mm x 1.07 mm x 0.90 mm voxel dimensions), and then reconstructed and reformatted on the axial plane with 560 x 560 x 220 matrix, 0.45 mm x 0.45 mm x 0.9 mm voxel dimensions, and without any inter-slice gap. These images are converted from DICOM (.dcm) to NIfTI (.nii.gz) format. Then are processed with FreeSurfer software (http://surfer.nmr.mgh.harvard.edu/): the 3D bone mask is subtracted in order to obtain the 3D reconstruction of the pial surface, the cortical ribbon volume and the parcellated and segmented brain volume based on the Desikan and Killiany atlas labeling [30] (Fig. 3.2);

- the post-implant 3D CT dataset, acquired with the O-arm System, Medtronic Inc. It's output dataset dimensions are 512 x 512 x 192 slices, with 0.4 x 0.4 x 0.8 anisotropic voxels. Starting from this dataset, the bone mask, computed by FreeSurfer, is subtracted resulting in the SEEG skull-stripped volume; the electrodes are automatically segmented through a gray scale thresholding (with the Grayscale Model Maker module in 3D Slicer) in order to obtain their 3D model (Fig. 3.3);

- a file that lists (list file) the models of intracerebral electrodes manufactured by Dixi Medical (Microdeep Intracerebral Electrodes®, Besançon, France). Each electrode has a fixed external diameter, contacts length and inter-leads gap, while the number of contacts, the electrode's length, the distance between adjacent groups of contacts, the number of contacts' groups and the number of leads per group vary depending on the electrode model; this file is the same for each patient's dataset of implanted electrodes;

- a FreeSurfer annotation file, containing the Brodmann areas labels: this is generated by mapping the PALS B12 Brodmann atlas [31] to the specific subject. Two color lookup tables, one for each hemisphere, are also created and placed in the Slicer ColorFiles folder; each row contains an index for the label, its name and its color in a RGB code;

- a patient file (.xml file) containing the list of all the electrodes present in a subject exploration, specifying for each one: the name (usually a letter from A to Z, associated to the exploration type), the model, the coordinates of the fiducials roughly placed by the user in the 3D Slicer scene after the implantation, expressed in the ijk image coordinate system. These fiducials represent the entry point (EP) of the electrode (located on the pial surface) and the target point (TP) as the tip of the electrode.

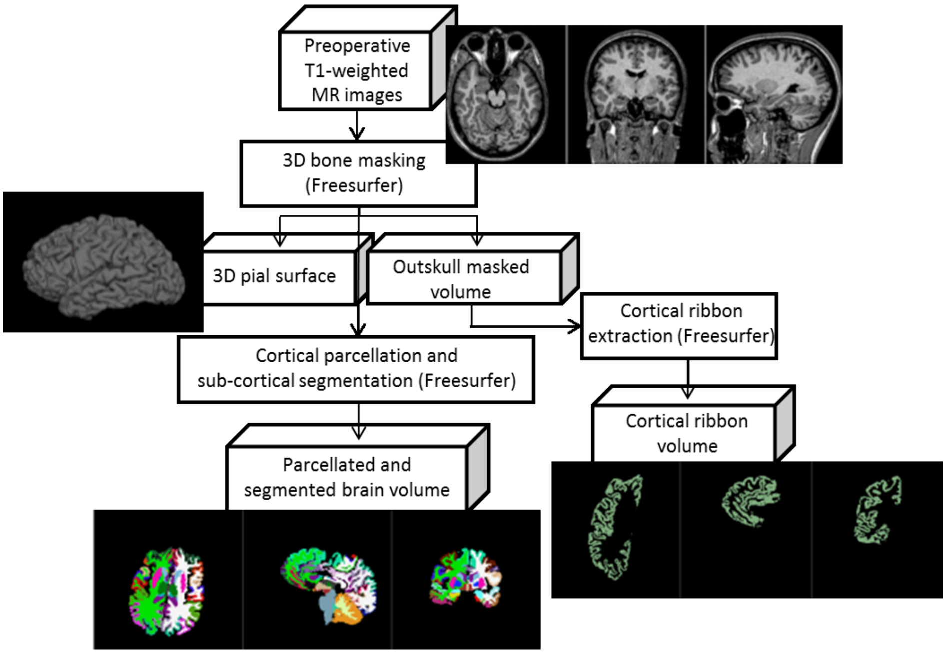

Figure 3.2: Image processing workflow starting from preoperative T1-weighted MR images for the extraction of the input data for the developed application.

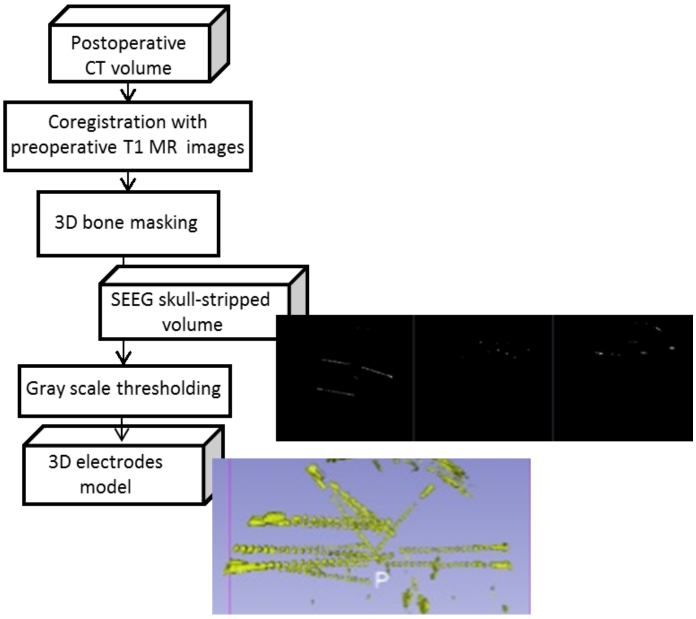

Figure 3.3: Image processing workflow starting from postoperative CT volume for the extraction of the input data for the developed application.

3.4 Electrodes reconstruction

Two methods of contacts localization and electrode reconstruction have been implemented. The first one, *Manual electrodes identification*, builds the contacts of the implanted electrode using a straight line with entry-target direction, on the basis of the electrode's model selected by the user. The second method, *Automatic electrodes identification*, automatically identifies contacts' centroids with an intensity-based analysis of the postoperative CT volume and then reconstructs the electrode's trajectory using a regression curve that fits them.

3.4.1 Manual electrodes identification

Input dataset This first method requires the 3D pial surface (from the preoperative processing) (Fig. 3.2), the SEEG skull-stripped volume and the 3D electrodes model (from the postoperative processing) (Fig. 3.3).

User-defined input data The user is asked to respectively localize the entry point (EP_user) of an electrode on the pial surface and its target point (TP_user), i.e. the electrode's tip. These points are identified in the Slicer 3D view by placing fiducials points on the model of the considered electrode (Fig. 3.4). The fiducials' coordinates are expressed in the RAS (Right, Anterior, Superior) coordinate system.

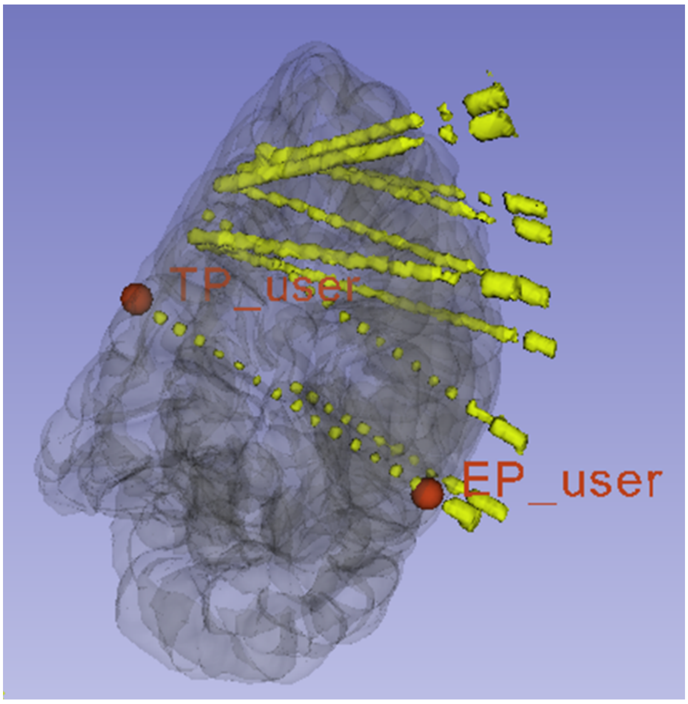

Figure 3.4: User-defined input data in the *Manual electrodes identification*. EP_user and TP_user are placed on the electrode 3D model; the positioning of the EP_point requires the 3D pial surface (in opacity).

The user is also asked to set the model of the electrode selecting it from the list file (as said, the listed models are those of the intracerebral electrodes manufactured by Dixi Medical). The possibility to insert a custom-made model is also given by specifying, using the horizontal sliders in the module interface, the number of contacts, the inter-contacts distance (li), the contacts length (lc), the inter-groups distance (lsi), the number of groups, the number of contact per each group and the distance between the electrode's tip and the distal contact (tipcont_dist) (this parameter is equal to zero for the electrodes manufactured by Dixi Medical) (Fig. 3.5).

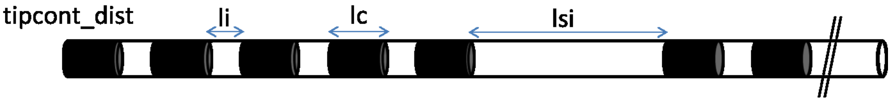

Figure 3.5: Schematic representation of an intracerebral electrode with groups of contacts. The inter-contacts distance (li), the contacts length (lc), the inter-groups distance (lsi) are highlighted in the figure. The tipcont_dist parameter (distance between the electrode's tip and the distal contact) is zero.

Algorithm Firstly, in order to find the name of the electrode being analyzed, for each electrode item of the patient file (containing the list of all the electrodes present in a subject exploration), the following steps are implemented:

1. Extraction of the x, y and z coordinates of the EP (ijk image reference system);
2. Transformation in RAS coordinates using the transformation matrix between the ijk image coordinate system and the RAS one;
3. Computation of the Euclidean distance of EP with the EP_user. The result is inserted into an array, with dimension equal to the number of electrodes, at the index corresponding to the item being considered.

Finally, in order to assign to the electrode being reconstructed the name it's associated with in the subject exploration, the array's index whose distance has the minimum value is found and the name of the electrode corresponding to the item with that index in the patient file is extracted.

Once the model of the electrode is specified by the user, its trajectory is reconstructed with EP_user-TP_user direction (**direction**):

$$\mathbf{direction} = \frac{\mathbf{EP\_user} - \mathbf{TP\_user}}{|\mathbf{EP\_user} - \mathbf{TP\_user}|}$$

Starting from the TP_user, the distal limit of the first contact is computed on the basis of the electrode specifications. If the tipcont_dist parameter is zero, the TP_user is the center of the distal contact; therefore the distal limit coordinates of the first contact are defined as (Fig. 3.6 (A)):

$$\mathbf{distal\,limit}(\mathbf{first\,contact}) = \mathbf{TP\_user} - 0.5 * lc * \mathbf{direction}$$

Instead, if tipcont_dist is not zero, i.e. the first contact is not on the electrode's tip (Fig. 3.6 (B)):

$$\mathbf{distal\,limit}(\mathbf{first\,contact}) = \mathbf{TP\_user} + tipcont\_dist * \mathbf{direction}$$

Then, the proximal limit coordinates of the 1st contact are computed as:

$$\mathbf{proximal\,limit}(\mathbf{first\,contact}) = \mathbf{distal\,limit}(\mathbf{first\,contact}) + lc * \mathbf{direction}$$

If there aren't groups of contacts or if the considered contact is not the first of a group (Fig. 3.6 (A and B)), the distal limit coordinates of the i-th lead are:

$$\mathbf{distal\,limit}(\mathbf{ith\,contact}) = \mathbf{proximal\,limit}((\mathbf{ith}-\mathbf{1})\,\mathbf{contact}) + li * \mathbf{direction}$$

Otherwise (Fig. 3.6 (C)):

$$\mathbf{distal\,limit}(\mathbf{ith\,contact}) = \mathbf{proximal\,limit}((\mathbf{ith}-\mathbf{1})\,\mathbf{contact}) + lsi * \mathbf{direction}$$

In general, the proximal limit coordinates of the i-th lead are:

$$\mathbf{proximal\,limit(ith\,contact)} = \mathbf{distal\,limit(ith\,contact)} + lc * \mathbf{direction}$$

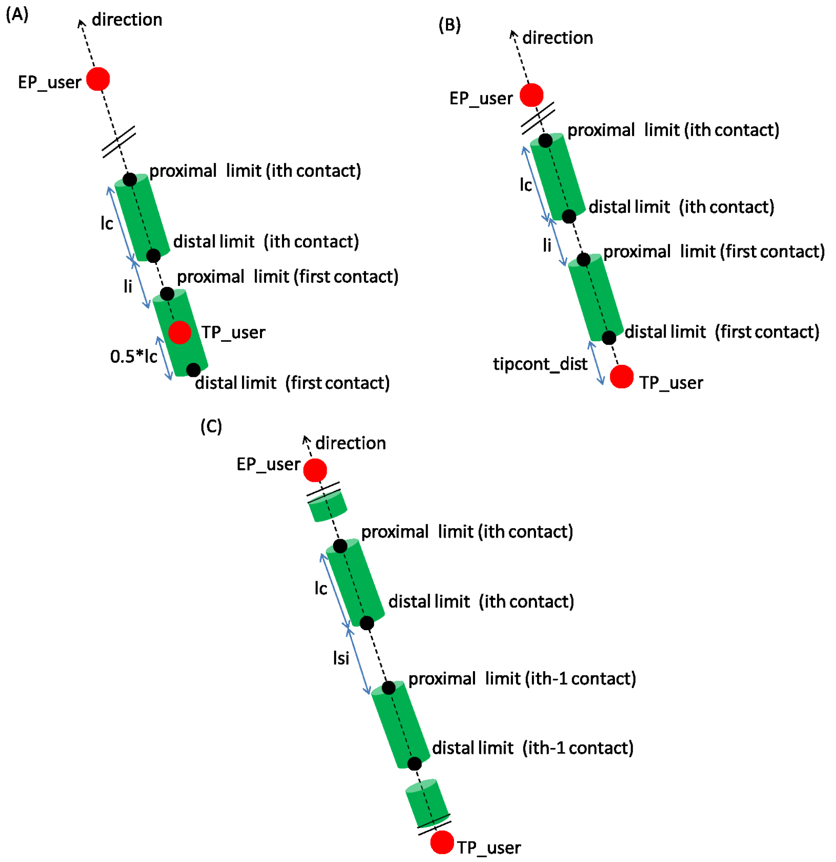

Figure 3.6: Schematic representation of the linear reconstruction of the electrode's contacts. (A): the tipcont_dist parameter is zero and groups of contacts are not present; (B): the tipcont_dist parameter is not zero and groups of contacts are not present; (C): the tipcont_dist parameter is zero and groups of contacts are present.

This method is used for all the contacts. Once the electrode's trajectory and contacts location are calculated, its visualization is implemented using the VTK library classes. The output of the *Manual electrodes identification* is the electrode's reconstruction from the target point to the entry point, highlighting contacts inside and outside the pial surface with different colors (Fig. 3.7). The *Manual electrodes identification* graphical user interface (GUI) is displayed in Fig. 3.8, the schematic flowchart of the algorithm is shown in Fig. 3.9.

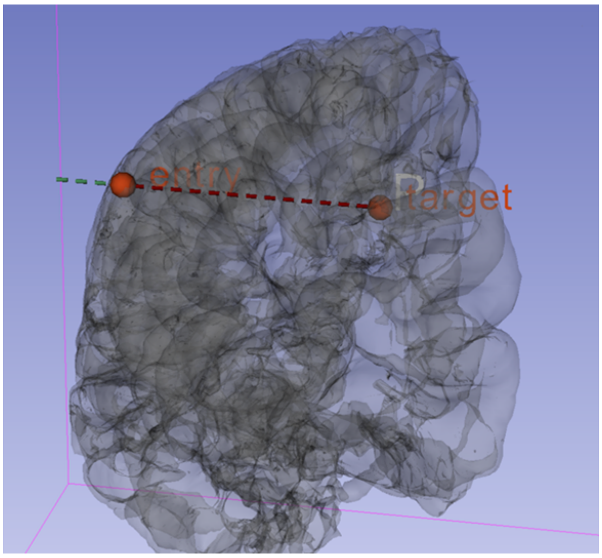

Figure 3.7: *Manual electrodes identification* output: the contacts inside the pial surface (in opacity) are displayed in red, while the ones outside are displayed in green.

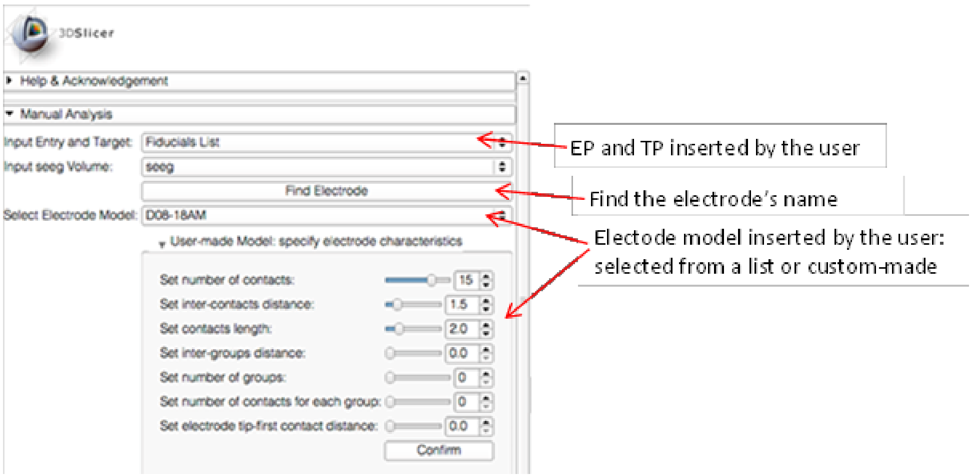

Input Entry and Target: Fiducials List
Input seeg Volume: seeg
Select Electrode Model: D08-18AM
Set number of contacts: 15
Set inter-contacts distance: 1.5
Set contacts length: 2.0
Set inter-groups distance: 0.0
Set number of groups: 0
Set number of contacts for each group: 0
Set electrode tip-first contact distance: 0.0

EP and TP inserted by the user

Find the electrode's name

Electode model inserted by the user: selected from a list or custom-made

Figure 3.8: The *Manual electrodes identification* GUI.

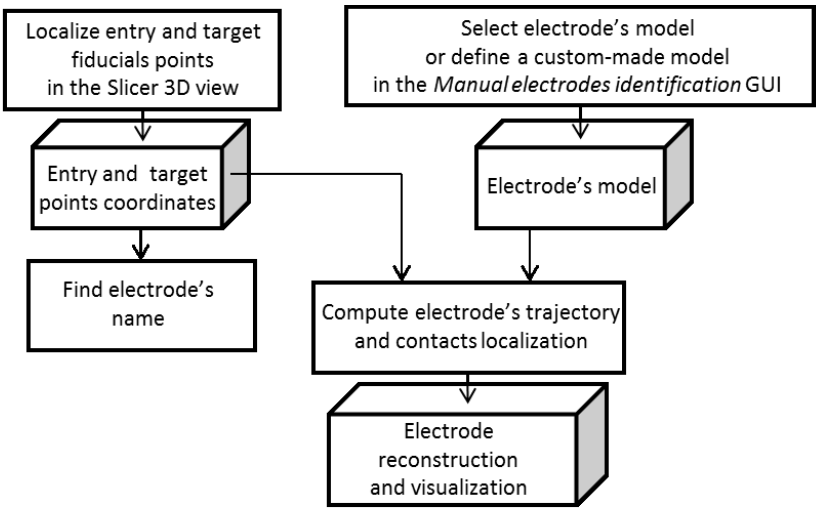

Figure 3.9: Flowchart of *Manual electrodes identification* algorithm.

3.4.2 Automatic electrodes identification

Input dataset The input data required by the algorithm is the SEEG skull-stripped volume (.nii.gz) from the postoperative CT.

User-defined input data The user selects the name of the electrode to be reconstructed from the list of the electrodes implanted in the considered patient (patient file).

Algorithm

(1) Automatic centroids identification For each electrode in the SEEG skull-stripped volume, an iterative algorithm finds the contacts' centroids. This algorithm is implemented in C++ and uses the ITK scientific library (Kitware, Clifton Park, NY, US); its pseudo-code is reported in Algorithm 3.1.

First, the entry point and the target point are extracted from the patient file. Next, a parametric line from target point to entry point, with voxel resolution, is initialized (Fig. 3.10 A).

Then, starting from target point and following the line's direction, a volume Region Of Interest (ROI) is built (Fig. 3.10 B); its dimension ($volumeROI\_size$) is defined in order to include a region greater than the contact. In particular, for each dimension i:

$$volumeROI\_size\,[i] = 2 * (image\,spacing\,[i] * 5 + 1)$$

where $image\,spacing$ is the voxel size in the dimension i.

Subsequently the moment of the ROI is computed. The image moment of (i+j+k) order is defined as the average intensity of the image voxels:

$$moment_{ijk} = \sum_x \sum_y \sum_z x^i y^j z^k I\,(x, y, z)$$

where x, y, z are the coordinates of each voxel in the ROI and $I(x, y, z)$ is the intensity of the SEEG skull-stripped volume in the voxel of x, y, z coordinates.

The ROI center of gravity is the new centroid. It is computed as:

$$\bar{x} = \frac{moment_{100}}{moment_{000}}, \ \bar{y} = \frac{moment_{010}}{moment_{000}}, \ \bar{z} = \frac{moment_{001}}{moment_{000}}$$

At each iteration along the line, the ROI is built only if a geometric constraint is fulfilled: the distance between the current voxel position on the line and the last identified centroid (I-CDist in Algorithm 3.1) must be comparable with the distance between adjacent contacts, i.e. with the contact length (Clength) and the inter-contacts gap (Cgap).

After having found the n-th contact centroid (where n is the number of contacts of the electrode's model), or having reached the entry point, the centroids coordinates are stored in an external .csv file.

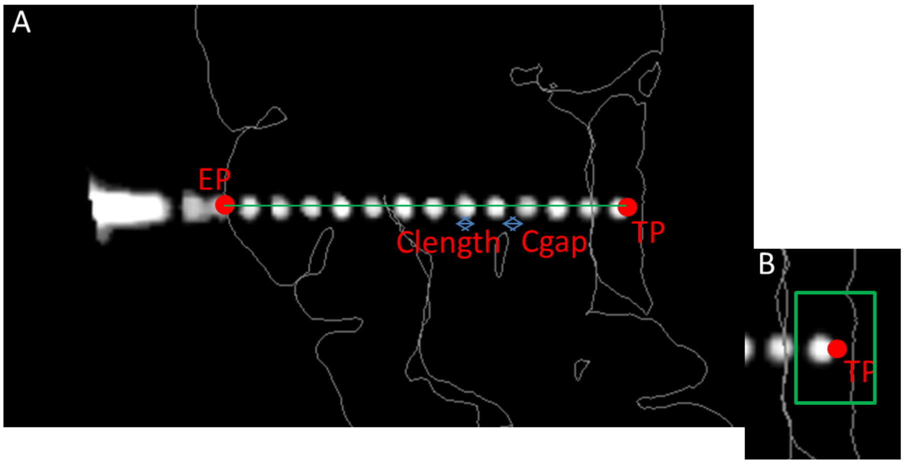

Figure 3.10: A schematic representation of the automatic centroids identification. A: electrode's contacts as appear in the SEEG skull-stripped volume and the pial surface in background are displayed. EP and TP are entry point and target point as reported in the patient file; the green line represents the parametric line initialized between TP and EP. B: the green box represent the ROI extracted around the TP, of which moment and center of gravity are computed.

Algorithm 3.1 Automatic centroids identification

```
path-> Initialize();
path-> AddVertex(target);
path-> AddVertex(entry);
contact=0;
for (iterator.GoToBegin(); iterator.IsAtEnd(); iterator++) do
    compute I-CDist;
    if (contact=0 or I-CDist >= Cgap+Clength-0.01)
        filter-> SetInput(seeg volume);
        filter-> SetRegionOfInterest(RegionAroundContact(iteratorIndex));
        calculator-> SetImage(filter->GetOutput());
        calculator-> GetMoment();
        for (i=0; i<3; i++) do
            centroid[i]= calculator-> GetCenterOfGravity()[i];
        end for
        contact++;
    end if
    if (contact=NumberOfContacts or iteratorIndex=entryIndex)
        break;
    end if
end for
```

(2) Centroids plane fitting According to the selected electrode's name, from the output file of **(1)**, the contacts centroids' coordinates are extracted and transformed from image coordinate system to RAS coordinate system ($centroids^{ras}$). Then the orthogonal distance regression plane, i.e. the plane that minimizes the sum of centroids squared distances to it, is computed using the Principal Components Analysis (PCA). The coefficients of the first two principal components ($1^{st}PC$ and $2^{nd}PC$) define vectors that form a basis for the plane. The third principal component ($3^{rd}PC$) is orthogonal to the first two, and its coefficients define the normal vector to the plane.

Using the VTK library, the best fit plane is represented in the Slicer scene (Fig. 3.11) and the $centroids^{ras}$ are projected on it ($proj\_centroids^{ras}$). Given the three principal components and the origin of the plane ($plane\_origin$), the transformation matrix T^{ras}_{plane} is calculated as:

$$T^{ras}_{plane} = \begin{bmatrix} 1^{st}PC & 2^{nd}PC & 3^{rd}PC & plane\_origin \\ 0 & 0 & 0 & 1 \end{bmatrix}$$

Through the T^{ras}_{plane} inverse, T^{plane}_{ras}, the coordinates of $proj_centroids^{ras}$are then expressed in the plane system of reference ($proj\_centroids^{plane}$):

$$\begin{bmatrix} proj\_centroids^{plane} \\ 1 \end{bmatrix} = T^{plane}_{ras} * \begin{bmatrix} proj\_centroids^{ras} \\ 1 \end{bmatrix}$$

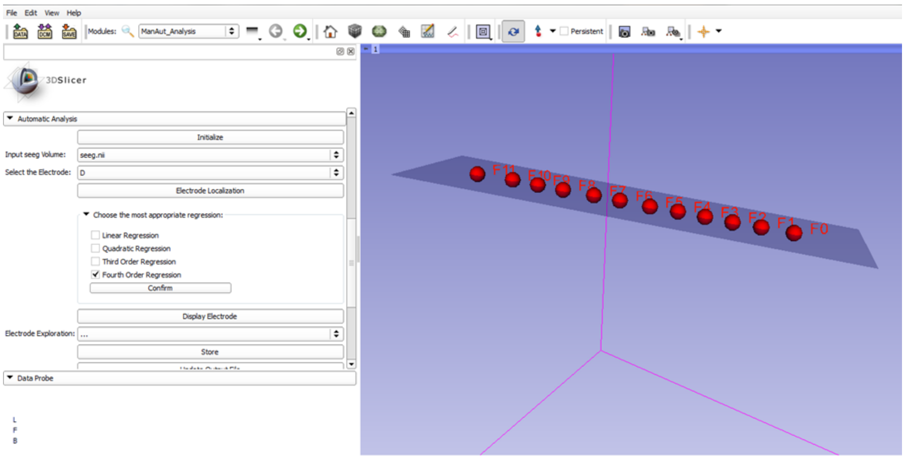

Modules: ManAut_Analysis

Automatic Analysis

Input seeg Volume: seeg.nii

Select the Electrode: D

Choose the most appropriate regression:

☐ Linear Regression
☐ Quadratic Regression
☐ Third Order Regression
☑ Fourth Order Regression

Electrode Exploration: ...

Figure 3.11: Fiducials points, as computed in the automatic centroids identification, and the orthogonal distance regression plane of the selected electrode are visualized in the Slicer 3D view.

(3) Curve fitting Using NumPy (Numerical Python), a package for scientific computing with Python, the first, second, third and fourth order polynomial regressions of the contacts centroids projected on the plane are implemented and successively visualized in the scene. The equations for the linear and quadratic polynomial curves are:

$$y_{proj\_centroids_i^{plane}} = \beta_0 x_{proj\_centroids_i^{plane}} + \beta_1$$

$$y_{proj\_centroids_i^{plane}} = \beta_0 x^2_{proj\_centroids_i^{plane}} + \beta_1 x_{proj\_centroids_i^{plane}} + \beta_2$$

where β_0, β_1, β_2 are the polynomial coefficients to be estimated.

The coefficient of determination R^2 for each of the previous regressions is computed as:

$$SS_{err} = \sum_{i=1}^{n} \left(y_{proj\_centroids_i^{plane}} - y_{reg\_centroids_i^{plane}} \right)^2$$

$$SS_{tot} = \sum_{i=1}^{n} \left(y_{proj\_centroids_i^{plane}} - \bar{y}_{proj\_centroids^{plane}} \right)^2$$

$$R^2 = 1 - \frac{SS_{err}}{SS_{tot}}$$

where $y_{reg\_centroids_i^{plane}}$ is the modeled value of the i-th centroid projected on the plane. SS_{err} measures the deviation of the y coordinates of the centroids projected on the plane from their modeled values, SS_{tot} measures the deviation of the y coordinates of the centroids projected on the plane from their mean.

Using the widget provided by the Qt library it is possible to report dynamic text on the GUI: in this case R^2 coefficients are displayed in the GUI module. The fitting curve associated with the highest value of R^2 is automatically checked, but the user has the option of changing and switching on each checkbox.

(4) Contacts reconstruction According to the selected polynomial regression order, the electrode's contacts are reconstructed with cylindrical shape taking into account the geometric characteristics of the corresponding electrode's model (Fig. 3.12). This last is retrieved, giving the electrode's name, from the patient file and its geometric specifications are assigned from the list file.

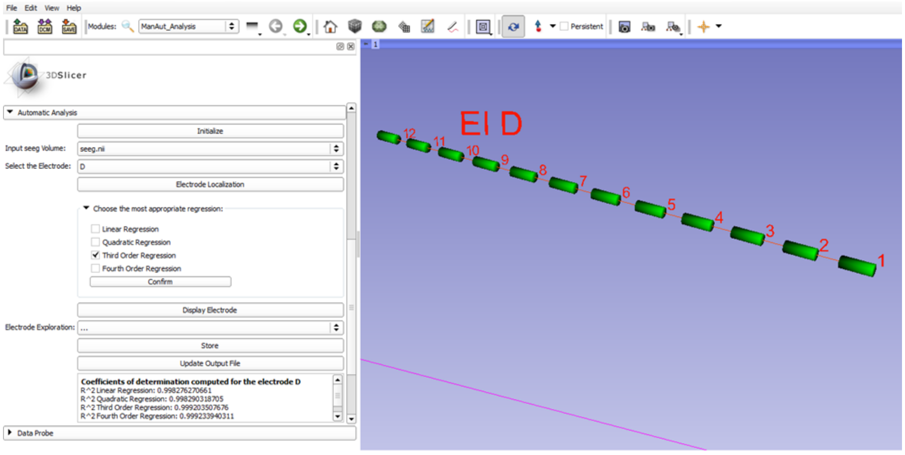

Modules: ManAut_Analysis

Input seeg Volume: seeg.nii

Select the Electrode: D

Choose the most appropriate regression:

☐ Linear Regression
☐ Quadratic Regression
☑ Third Order Regression
☐ Fourth Order Regression

Confirm

Electrode Exploration: ...

```
Coefficients of determination computed for the electrode D
R^2 Linear Regression: 0.998276270661
R^2 Quadratic Regression: 0.998290318705
R^2 Third Order Regression: 0.999203507676
R^2 Fourth Order Regression: 0.999233940311
```

Figure 3.12: On the left, the module GUI displaying the R^2 coefficients of the polynomial regressions and the curve's order checked by the user. On the right, the reconstruction with a 3rd order regression curve of the labeled contacts of the selected electrode, is shown in the Slicer 3D view.

The schematic flowchart of the algorithm is shown in Fig 3.13.

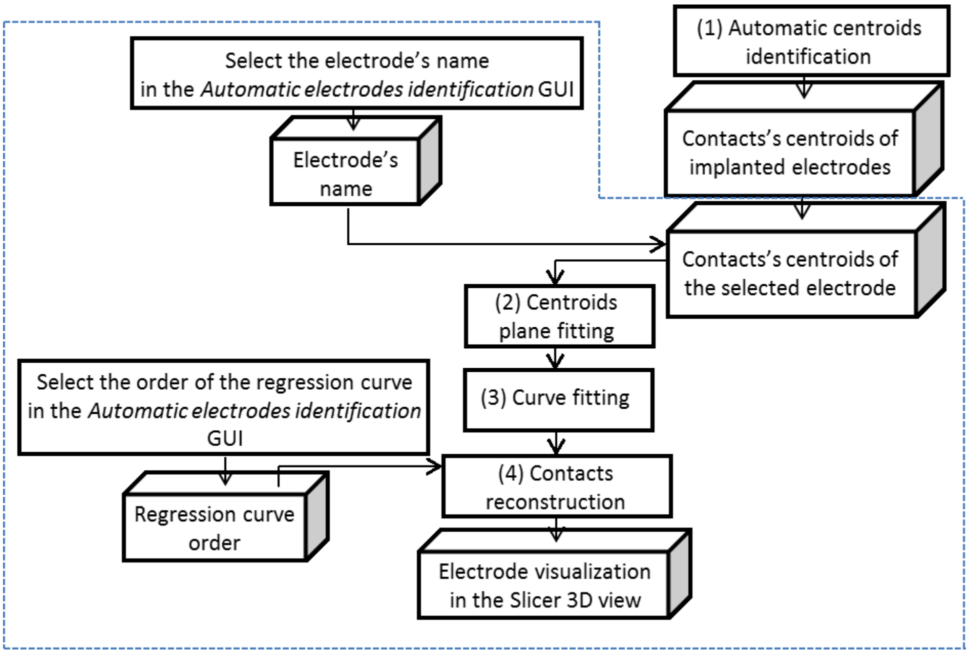

Figure 3.13: Flowchart of *Automatic electrodes identification* algorithm. The dashed box embodies the steps executed for each electrode.

3.5 Electrodes exploration

Once the electrode has been reconstructed and visualized in the Slicer 3D view, the position of each contact with respect to the cerebral gray matter, the regions from the Desikan and Killiany atlas and the Brodmann areas, is extracted.

Input dataset The required input data are (Fig. 3.14):

- the left and right pial surfaces (.vtk), if the exploration is bilateral, or one of them if it's unilateral, from the preoperative MR images;
- the FreeSurfer annotation file, containing the Brodmann areas labels. It has to be loaded as scalar overlay on the pial surface model; at the same time the color lookup table assigned to this scalar should be active and visible;
- the parcellated and segmented brain volume (.nii.gz) based on the Desikan and Killiany atlas labeling from the preoperative MR images. Each row of the corresponding color lookup table contains an index for a Desikan and Killiany atlas region, the region name and the region color in a RGB code;
- the left and/or right cortical ribbon volume (.nii.gz) from the preoperative MR images.

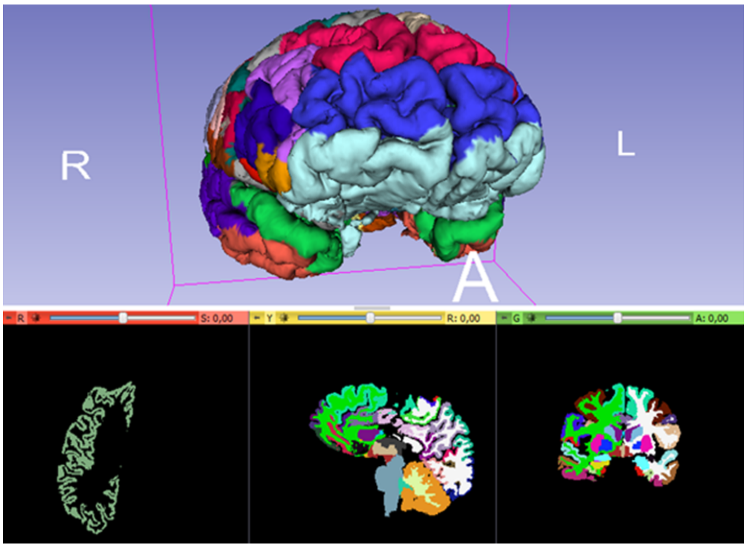

Figure 3.14: Electrodes exploration input data. The left and right pial surfaces with the FreeSurfer annotation files loaded as scalars are shown in the Slicer 3D view. In the axial view (red) the right cortical ribbon volume is visualized, while in the sagittal (yellow) and coronal (green) views the parcellated and segmented brain volume based on the Desikan and Killiany atlas is displayed.

User-defined input data The user selects, from a popup list in the GUI module, the type of exploration he/she's interested in.

Algorithm If the *Gray Matter* option is selected, the cortical ribbon volume is used to discriminate among cortical contacts, inside the gray matter, and no cortical contacts. The cortical ribbon volume is a binary volume mask of the cortical ribbon, i.e., each voxel is either 1 or 0 depending upon whether it falls in the ribbon or not. For each point of the cylindrical-shaped contact of the reconstructed electrode, its position within the cortical ribbon volume is investigated: in particular, it is checked if the scalar value of the corresponding volume voxel is 1 or not. Just one point of the cylinder with value equal to 1 is sufficient to consider the investigated contact belonging to the gray matter.

Otherwise, if the user selects the *Desikan and Killiany atlas* choice, a procedure similar to the one described above is implemented. The parcellated and segmented brain volume is the segmentation of the preoperative T1-weighted MR images according to the Desikan and Killiany atlas. It is a label map volume, i.e., each voxel is associated with a number indicating the neuroanatomical region at its location (based on its color lookup table). Once for each reconstructed electrode's contact the crossed neuroanatomical regions are identified (according to the contact's points location in the volume), these are reconstructed and displayed in the 3D Slicer scene (Fig. 3.15).

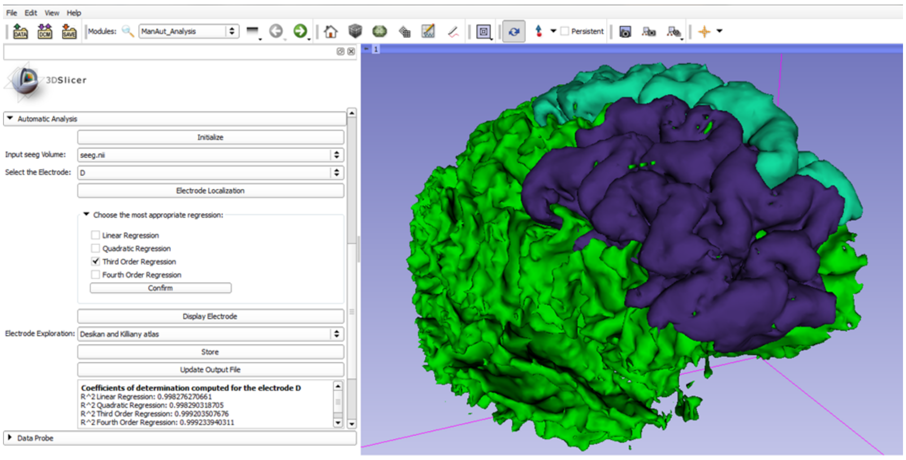

Modules: ManAut_Analysis

Input seeg Volume: seeg.nii

Select the Electrode: D

Choose the most appropriate regression:

☐ Linear Regression
☐ Quadratic Regression
☑ Third Order Regression
☐ Fourth Order Regression

Electrode Exploration: Desikan and Killiany atlas

```
Coefficients of determination computed for the electrode D
R^2 Linear Regression: 0.998276270661
R^2 Quadratic Regression: 0.998290318705
R^2 Third Order Regression: 0.999203507676
R^2 Fourth Order Regression: 0.999233940311
```

Figure 3.15: Visualization of the Desikan and Killiany regions crossed by the electrode in the Slicer 3D view after the user selection of the *Desikan and Killiany atlas* option in the drop down menu.

The last option of the drop down list is *PALS B12 Brodmann atlas.* The Brodmann areas are loaded as scalars values on the pial surface (see Fig. 3.14, in the Slicer 3D view). For each point of the analyzed electrode this scalar value is extracted and, from the associated look up table, the corresponding label name of the Brodmann area is derived.

Once the information about the exploration of the considered electrode are collected, a .csv file is automatically generated or, if it already exists, is automatically updated. This file reports, for each studied electrode:

- the list of its contacts;
- the discrimination between cortical or no cortical contacts;
- the neuroanatomical regions, based on the Desikan and Killiany atlas, that each contact goes through. If the contact is located outside the pial surface, this remark is stored;
- the list of Brodmann areas crossed along the entire electrode's trajectory.

3.6 Experimental protocol and data analysis

The analysis was conducted on 19 patients who underwent SEEG at "Claudio Munari" Center for Epilepsy and Parkinson Surgery, Niguarda Ca' Granda Hospital, Milan, Italy. Patients description is summarized in Table 3.1 (patient index, age, SEEG exploration pattern, hemisphere side, number of electrodes for each exploration). A population of 242 electrodes was analyzed.

# Patient	Age	Pattern	Side	# Electrodes
1	31	Frontal	Left	10
2	9	Fronto-temporal	Left	13
3	21	Fronto-central	Bilateral	14
4	17	Temporo-posterior	Left	15
5	28	Temporo-posterior	Right	14
6	36	Temporo-posterior	Right	14
7	21	Central	Right	9
8	32	Fronto-temporal	Left	14
9	18	Fronto-central	Right	14
10	18	Frontal	Bilateral	12
11	34	Temporo-insulo perisylvian	Left	14
12	44	Fronto-temporal	Right	13
13	27	Temporo-insulo perisylvian	Right	12
14	28	Fronto-temporal	Right	14
15	19	Temporo-insulo perisylvian	Right	15
16	27	Temporo-insulo perisylvian	Right	12
17	26	Frontal	Right	12
18	32	Fronto-temporal	Left	16
19	16	Frontal	Left	14

Table 3.1: Patients characteristics. Pattern indicates the topographical region explored by most of the electrodes.

The first test determines the order of the regression curve that will be used for the reconstruction of electrodes contacts in the subsequent analysis.

Electrode curve modelling In order to determine the best degree of the polynomial regression curve that models the electrode trajectory, the Euclidean distance between the contacts centroids positions ($centroids^{ras}$), found with the automatic centroids identification, and the corresponding regression points ($reg\_centroids^{ras}$) was computed for the polynomial curves of orders 1st, 2nd, 3rd and 4th (Fig. 3.16).

The non-parametric Kruskal-Wallis test (p-value$<$0.05) with the Bonferroni correction was performed to compare the 4 distance populations. The statistical analysis was performed using MATLAB 7.11.0 (®2010b) and it was conducted for 4 patients, i.e. 50 electrodes and 679 contacts overall.

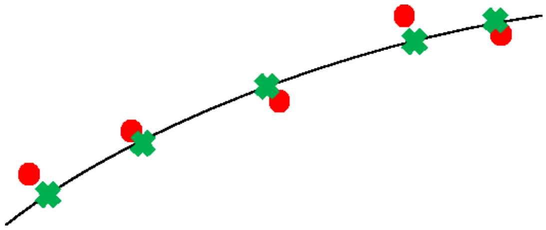

Figure 3.16: Schematic representation of the Electrode curve modelling analysis. Red circles represent the contacts centroids positions as found with the automatic centroids identification, while green crosses represent the corresponding points on the regression curve.

Electrodes identification accuracy A second analysis was carried out to validate and evaluate the accuracy of the two methods: *Manual electrodes identification* (b) and *Automatic electrodes identification* (c) (3rd order regression). For this purpose, a gold standard (a) identified on the postoperative SEEG skull-stripped volume was considered. To obtain this latter, the surgeon has been asked to indicate, as precisely as possible, the contacts centroids, by placing a fiducial in the center of the contacts artifact on the orthogonal views of the postoperative CT volume in 3D Slicer. For all the 19 patients, a subset of 3 electrodes was considered, i.e. 820 contacts total. The Euclidean distance between corresponding centroids' leads found as gold standard and respectively the ones detected with the *Manual electrodes identification* and *Automatic electrodes identification* was computed.

The non-parametric Wilcoxon test (p-value$<$0.05) was performed in MATLAB®.

Electrode exploration analysis This study was performed with the objective of verifying if a correlation exists between:

1. The exploration pattern and the Desikan and Killiany atlas regions crossed by the contacts; thus, patients were grouped according to their clinical pattern (Fig. 3.17) and the number of contacts crossing each Desikan and Killiany atlas region was counted.
2. The exploration pattern and the FreeSurfer available Brodmann areas that the electrodes go through; to do this, patients were grouped according to their pattern and the number of electrodes crossing each FreeSurfer available Brodmann area was counted.
3. The Brodmann area at the entry point of the electrode on the pial surface and the Desikan and Killiany segmented regions crossed by the contacts during its trajectory. Therefore, considering each Brodmann area crossed by the electrodes entering inside the pial surface, the number of contacts crossing each Desikan and Killiany atlas region was counted.

Electrode curvature analysis The last analysis was carried out in order to investigate a possible correlation between the electrode's mean curvature (out-

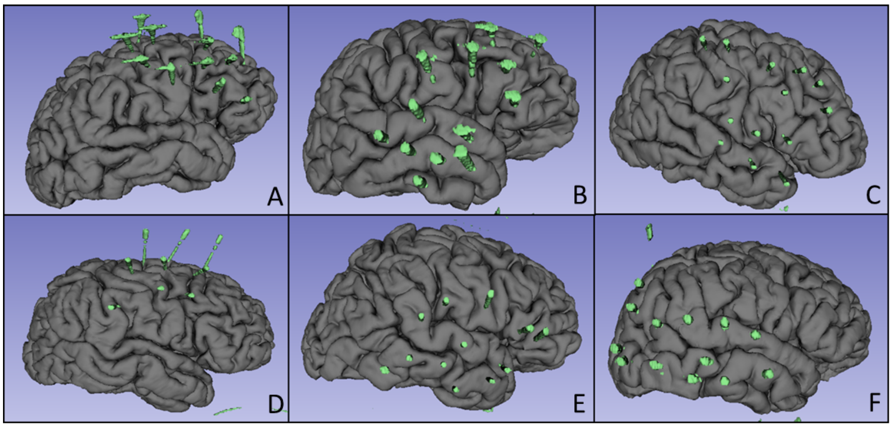

Figure 3.17: Exploration patterns examples. In the upper row, starting from left, the following pattern are represented: frontal (A), fronto-temporal (B) and fronto-central (C); while, at the bottom, central (D), temporo-insulo perisylvian (E) and temporo-posterior (F) patterns are displayed.

come variable) and several explanatory variables. In particular, the explanatory variables considered in the study are:

- the electrode's intracerebral length, computed as the Euclidean distance between the target point and the entry point, as reported in the patient file;
- the electrode's insertion angle with respect to the skull, defined as the incidence acute angle between the electrode's trajectory and the normal vector to the skull surface at the entry point (Fig. 3.18). In order to obtain this variable, the model of the skull of each patient was generated starting from a preoperative CT volume and applying a gray scale thresholding;
- the Desikan and Killiany atlas regions crossed by the electrode.

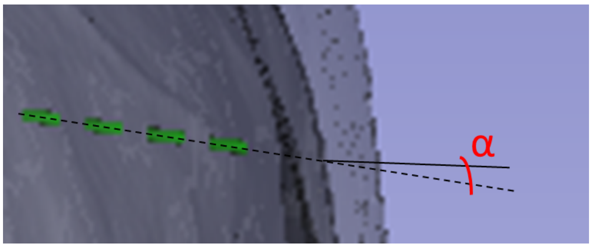

Figure 3.18: Schematic representation of the electrode's insertion angle (α) with respect to the skull. The dotted line represents the electrode's trajectory, while the continuous one represents the local normal vector to the skull surface.

Given the explicit formula of the third order polynomial regression curve,

$$y_{reg\_centroids_i^{plane}} = \hat{\beta}_0 x^3_{proj\_centroids_i^{plane}} + \hat{\beta}_1 x^2_{proj\_centroids_i^{plane}} + \hat{\beta}_2 x_{proj\_centroids_i^{plane}} + \hat{\beta}_3$$

where $\hat{\beta}_0$, $\hat{\beta}_1$, $\hat{\beta}_2$ are the estimated polynomial coefficients, an index corresponding to the mean curvature along the electrode axis [32] was computed. In particular, a Local Curvature Index (LCI) is computed as:

$$LCI = \frac{\left| y''_{reg\_centroids^{plane}} \right|}{\left(1 + \left(y'_{reg\_centroids^{plane}}\right)^2\right)^{3/2}}$$

Then, it is averaged over the entire curve's length in order to obtain the Mean Curvature Index (MCI):

$$MCI = \frac{1}{n} \sum_{i=1}^{n} LCI(i)$$

with n the number of regression points.

After the collection of these quantities for all the patients, a multivariate analysis was performed fitting a mixed effects linear regression model on a dataset of 242 electrodes, considering MCI as outcome variable. A random "patient ID" effect was included into the model to account for the electrodes implanted in the same subject, leading to correlated observations. P-value <0.05 was considered. The statistical analysis was executed using R 2.15.

Table 3.2 summarizes the outcome variable and the explanatory variables used in the multivariate analysis. Values of the numerical variables, i.e. MCI, length and skull angle are not normally distributed (the p-value of the Shapiro-Wilk normality test is, respectively, $<$ 2.2e-16, 0.0001 and 3.858e-05). Each Desikan and Killiany atlas region is considered as binary variable: the value assigned in the model is 1 or 0 depending if it is crossed by the considered electrode or not.

Outcome variable			
	NUMERICAL VARIABLE		
	Median		IQR
MCI	0.002		0.001 - 0.004
Explanatory variables			
	NUMERICAL VARIABLES		
	Measure unit	Type	Median (IQR)
Length	mm	Continuos	46.075 (33.255 - 52.844)
Skull angle	degrees	Continuos	25.366 (14.483 - 36.580)
	CATEGORICAL VARIABLES		
			Categories
Desikan and Killiany atlas region			1
			0

Table 3.2: Outcome variable and explanatory variables considered in the multivariate analysis.

Chapter 4

Results

This chapter illustrates the outputs of the four analysis (electrode curve modelling, electrodes identification accuracy, electrode exploration analysis, electrode curvature analysis) presented in Section 3.6 of Chapter 3.

4.1 Electrode curve modelling

Fig. 4.1 shows the Euclidean distance between the contacts centroids positions, found with the automatic centroids identification (3.4.2), and the corresponding regression points, for the polynomial curves of orders 1st, 2nd, 3rd and 4th. The reported values represent the median of the computed distances for each degree of the polynomial regression curve and the interval between the first and the third quartile, the inter-quartile range (IQR) (see Table 4.1). The histogram shows a decreasing distance as the regression order increases: the higher the degree of the polynomial, the better the modelling. A statistically significant difference was found between the first order and the third order polynomial regression curves, between the first order and the fourth order polynomial regression curves and between the second order and the fourth order polynomial regression curves. Therefore, the third order polynomial was chosen as regression curve for the further analysis.

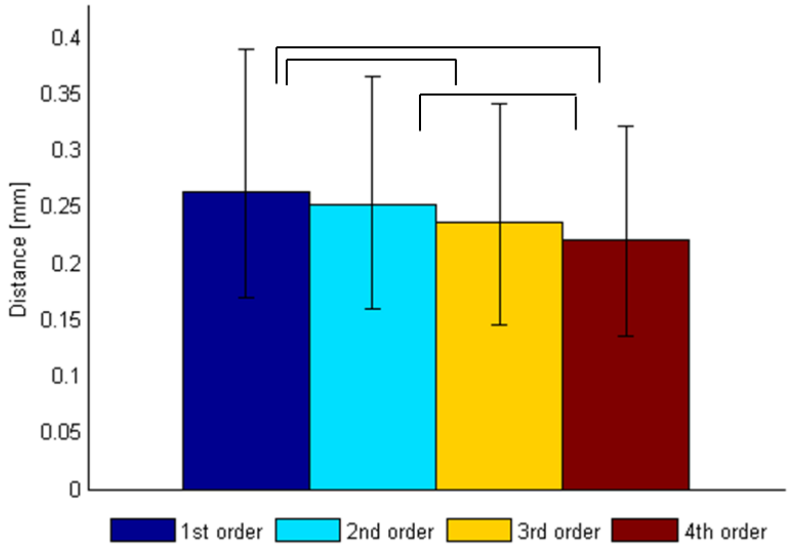

Figure 4.1: Electrode curve modelling. Vertical bars indicate the inter-quartile range; horizontal bars indicate a statistically significant difference. The p-value of the Kruskal-Wallis test is 4.182e-009.

Polynomial order	Median distance (IQR) [mm]
1	0.263 (0.220)
2	0.252 (0.206)
3	0.237 (0.197)
4	0.221 (0.186)

Table 4.1: Median and IQR of the Euclidean distances between the contacts centroids positions, found with the automatic centroids identification, and the corresponding regression points, for the 1st, 2nd, 3rd and 4th order regression curves.

4.2 Electrodes identification accuracy

This analysis was performed in order to determine the accuracy of the *Manual electrodes identification* (b) and *Automatic electrodes identification* (c) algorithms. The spatial accuracy of these two methods was validated using the postoperative CT volume, where each contact of the 57 considered electrodes (3 for each subject) was manually identified (a). Fig. 4.2 displays the Euclidean distance value (median and IQR) between contacts centroids position, as determined by (b) and (c) with respect to the one identified by (a). The contacts centroids of the electrodes reconstructed with the *Manual electrodes identification* have a greater distance from the considered gold standard (median 1.018 mm, IQR 0.494 mm) compared to the ones reconstructed with the *Automatic electrodes identification* (median 0.529 mm, IQR 0.384 mm) (Table 4.2).

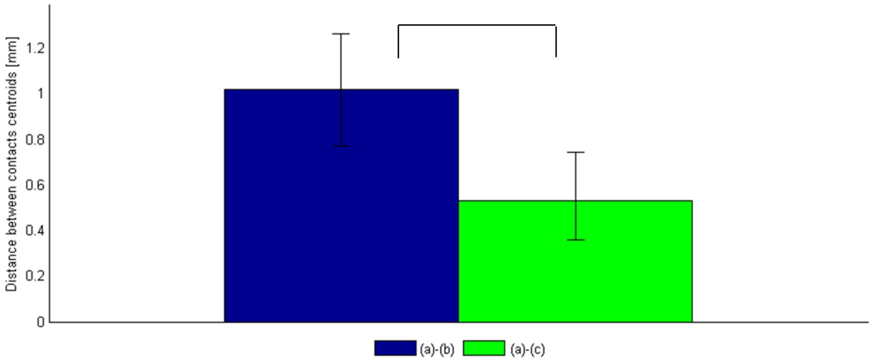

Figure 4.2: Comparison between the distances to the gold standard from respectively the centroids computed with the *Manual electrodes identification* algorithm and the ones computed with the *Automatic electrodes identification* algorithm. Vertical bars indicate the inter-quartile range; horizontal bar indicates a statistically significant difference. The p-value of the Wilcoxon rank sum test is <0.0001.

Comparison	Median (IQR) [mm]
(a)-(b)	1.018 (0.494)
(a)-(c)	0.529 (0.384)

Table 4.2: Median (IQR) of the Euclidean distances between contacts centroids as reconstructed with *Manual electrodes identification* (b) and *Automatic electrodes identification* (c) methods, with respect to the ones manually identified (a).

Fig. 4.3 displays the reconstruction of a not visually deviated electrode and of a visually deviated one using the *Manual electrodes identification* and the *Automatic electrodes identification* methods. Fig. 4.4 and Table 4.3 show the Euclidean distance value (mean and IQR) between contacts centroids as reconstructed with the two algorithms (b and c), with respect to the ones manually identified (a), when considering only a visually deviated 18 leads electrode.

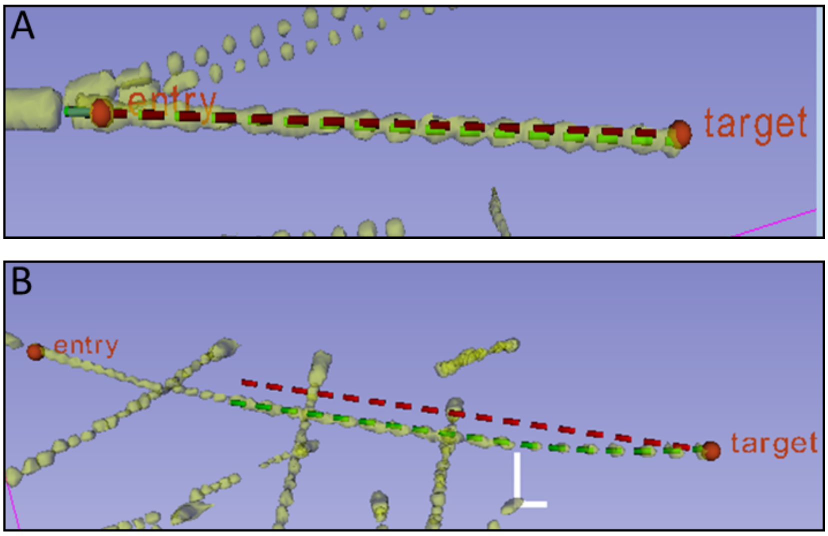

Figure 4.3: Reconstruction of a not visually deviated electrode (A) and of a visually deviated electrode (B) using the *Manual electrodes identification* (red) and the *Automatic electrodes identification* (green).

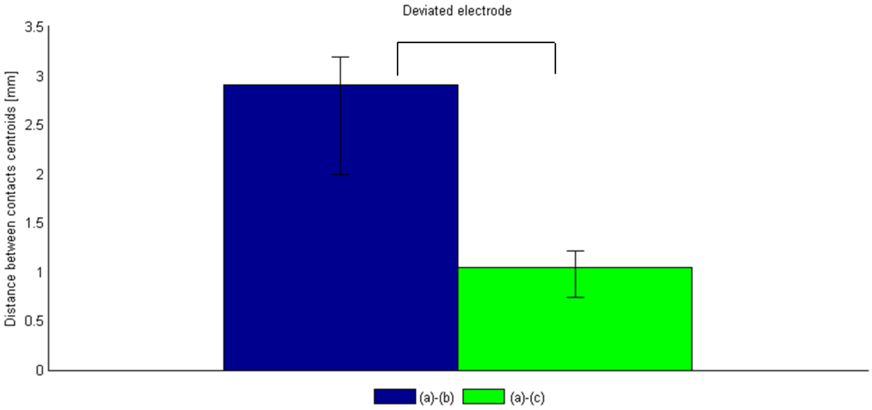

Figure 4.4: Comparison between *Manual electrodes identification* and *Automatic electrodes identification* algorithms when considering only a visually deviated electrode. Vertical bars indicate the inter-quartile range; horizontal bar indicates a statistically significant difference. The p-value of the Wilcoxon rank sum test is 2.6229e-006.

Comparison	Median (IQR) [mm]
(a)-(b)	2.913 (1.202)
(a)-(c)	1.053 (0.479)

Table 4.3: Median (IQR) of the Euclidean distances between contacts centroids as reconstructed with *Manual electrodes identification* (b) and *Automatic electrodes identification* (c) methods, with respect to the ones identified by the gold standard (a), when considering only a visually deviated 18 leads electrode.

4.3 Electrode exploration analysis

Fig. 4.5 represents color coded values of the total number of contacts, considering all the subjects belonging to a specific pattern, that crossed a specific Desikan and Killiany atlas region, divided by the number of patients that share this pattern. The regions of the Desikan and Killiany atlas were classified based on the belonging lobe, according to [30]. In Fig. 4.6 there is the same information differently represented: in particular, in each histogram, mean and standard deviation of the number of contacts exploring an atlas region, grouping patients according to their pattern, are displayed (see Table 4.4).

Fig. 4.7 displays color coded values of the total number of electrodes, considering all the subjects belonging to a specific pattern, that crossed a specific Brodmann area, divided by the number of patients that share this pattern; even in this case the Brodmann were classified based on the lobe they belong. In Fig. 4.8 there is the same information differently represented.

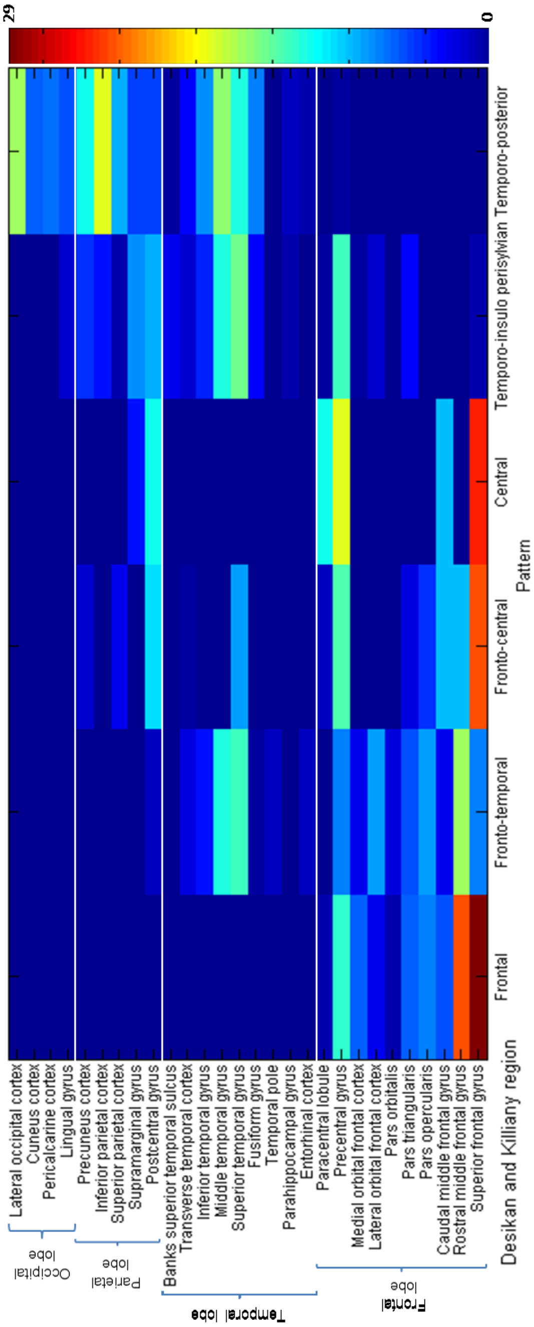

Figure 4.5: Correlation between the explored pattern and the Desikan and Killiany atlas regions crossed by the implanted electrodes contacts.

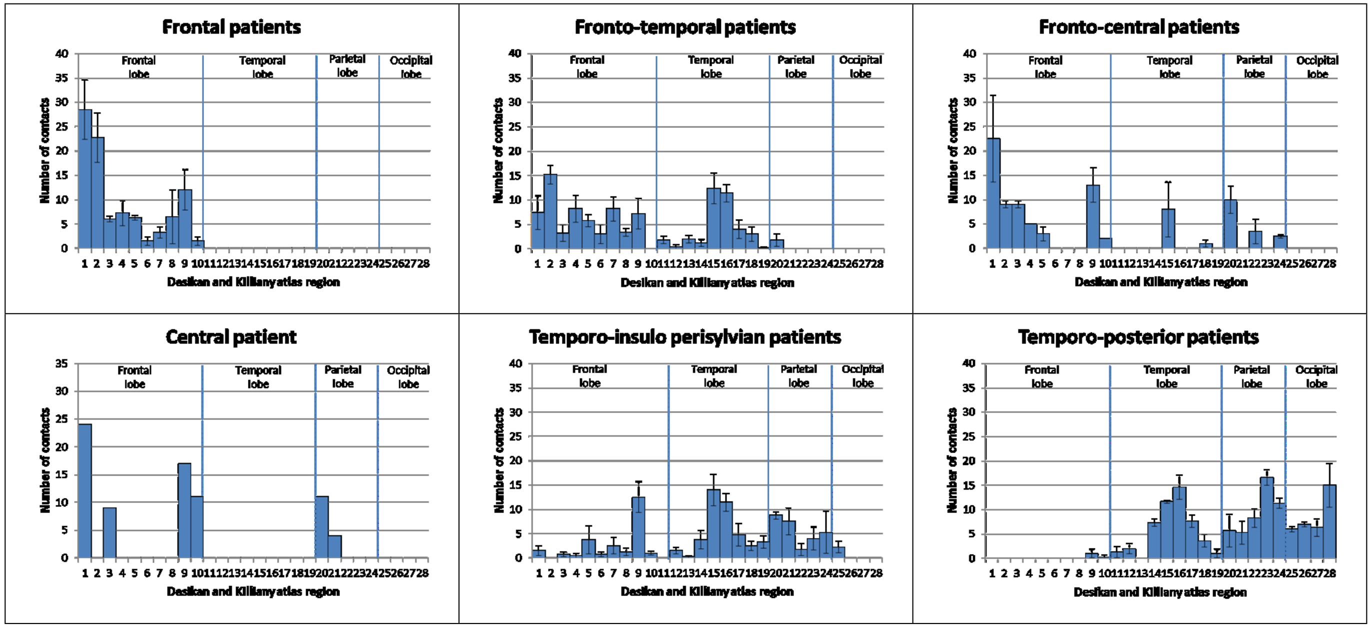

Figure 4.6: Distribution of electrodes contacts in the Desikan and Killiany atlas regions according to the exploration pattern. In each histogram the mean and the standard deviation (SD) values of the number of contacts crossing a specific Desikan and Killiany atlas region, considering all patients belonging to the analyzed pattern, are displayed.

Desikan and Killiany atlas region	F	FT	FC	C	TIP	TP
	Mean(SD)	Mean(SD)	Mean(SD)		Mean(SD)	Mean(SD)
Superior frontal gyrus	28.5(12.12)	7.4(6.91)	22.5(17.68)	24	1.5(1.91)	0(0)
Rostral middle frontal gyrus	22.75(10.14)	15,2(3.83)	9(1.41)	0	0(0)	0(0)
Caudal middle frontal gyrus	6(1.15)	3.2(3.27)	9(1.41)	9	0.75(0.96)	0(0)
Pars opercularis	7.25(5.19)	8.2(5.54)	5(0)	0	0.5(1)	0(0)
Pars triangularis	6.25(0.96)	5.8(2.59)	3(2.83)	0	3.75(5.68)	0(0)
Pars orbitalis	1.5(1.73)	3(3.74)	0(0)	0	0.75(0.96)	0(0)
Lateral orbital frontal cortex	3.25(2.36)	8.2(4.92)	0(0)	0	2.5(3.32)	0(0)
Medial orbital frontal cortex	6.5(11.09)	3.4(1.52)	0(0)	0	1.25(1.5)	0(0)
Precentral gyrus	12(8.29)	7.2(6.22)	13(7.07)	17	12.5(6.35)	1(1.73)
Paracentral lobule	1.5(1.73)	0(0)	2(0)	11	1(0.82)	0.33(0.58)
Entorhinal cortex	0(0)	1.8(1.48)	0(0)	0	0(0)	1.33(2.31)
Parahippocampal gyrus	0(0)	0.4(0.89)	0(0)	0	1.5(1.29)	2(2)
Temporal pole	0(0)	2(1.58)	0(0)	0	0,.5(0.5)	0(0)
Fusiform gyrus	0(0)	1.2(1.30)	0(0)	0	3.75(3.77)	7.33(1.53)
Superior temporal gyrus	0(0)	12.4(6.23)	8(11.31)	0	14(6.38)	11.67(0.58)
Middle temporal gyrus	0(0)	11.4(3.58)	0(0)	0	11.5(3.70)	14.67(4.93)
Inferior temporal gyrus	0(0)	4(3.81)	0(0)	0	4.75(4.65)	7.67(2.52)
Transverse temporal gyrus	0(0)	3(3)	1(1.41)	0	2.5(1.91)	3.67(2.52)
Banks superior temporal cortex	0(0)	0.2(0.45)	0(0)	0	3.25(2.5)	1(1.73)
Postcentral gyrus	0(0)	1.8(2.49)	10(5.66)	11	8.75(1.5)	5.67(6.66)
Supramarginal gyrus	0(0)	0(0)	0(0)	4	7.5(5.51)	5.33(4.73)
Superior parietal cortex	0(0)	0(0)	3.5(4.95)	0	1.75(2.36)	8.33(3,79)
Inferior parietal cortex	0(0)	0(0)	0(0)	0	4(4.69)	16.67(3.21)
Precuneus cortex	0(0)	0(0)	2.5(0.71)	0	5.25(8.62)	11.33(2.08)
Lingual gyrus	0(0)	0(0)	0(0)	0	2.25(2.22)	6(1)
Pericalcarine cortex	0(0)	0(0)	0(0)	0	0(0)	7(1)
Cuneus cortex	0(0)	0(0)	0(0)	0	0(0)	6.33(3.51)
Lateral occipital cortex	0(0)	0(0)	0(0)	0	0(0)	15(9)

Table 4.4: Mean(SD) of the number of contacts crossing a Desikan and Killiany atlas region considering patients grouped according to their exploration pattern (F: frontal; FT: fronto-temporal; FC: fronto-central; C: central; TIP: temporo-insulo perisylvian; TP: temporo-posterior).

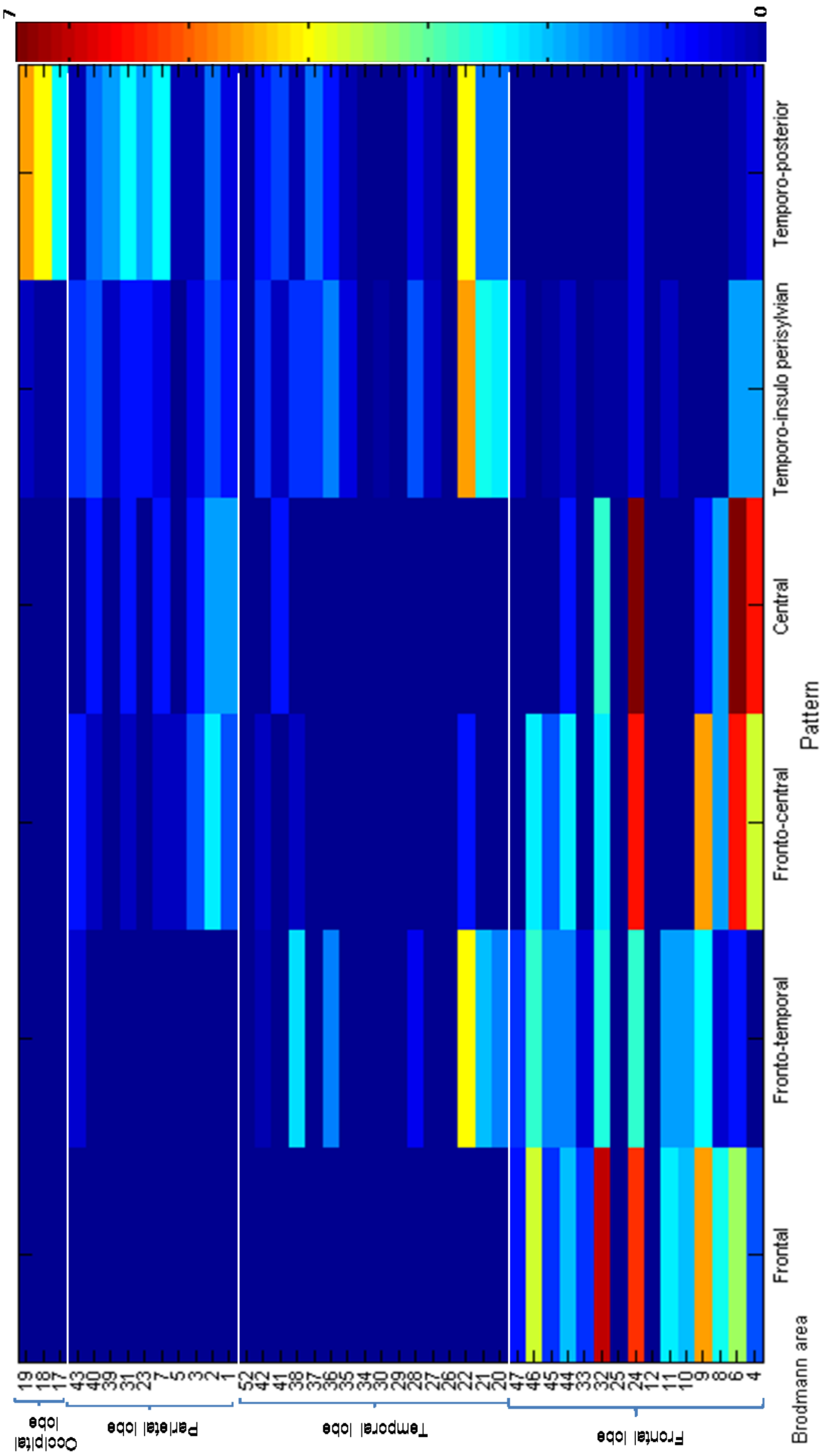

Figure 4.7: Correlation between the explored pattern and the Brodmann areas crossed by the implanted electrodes.

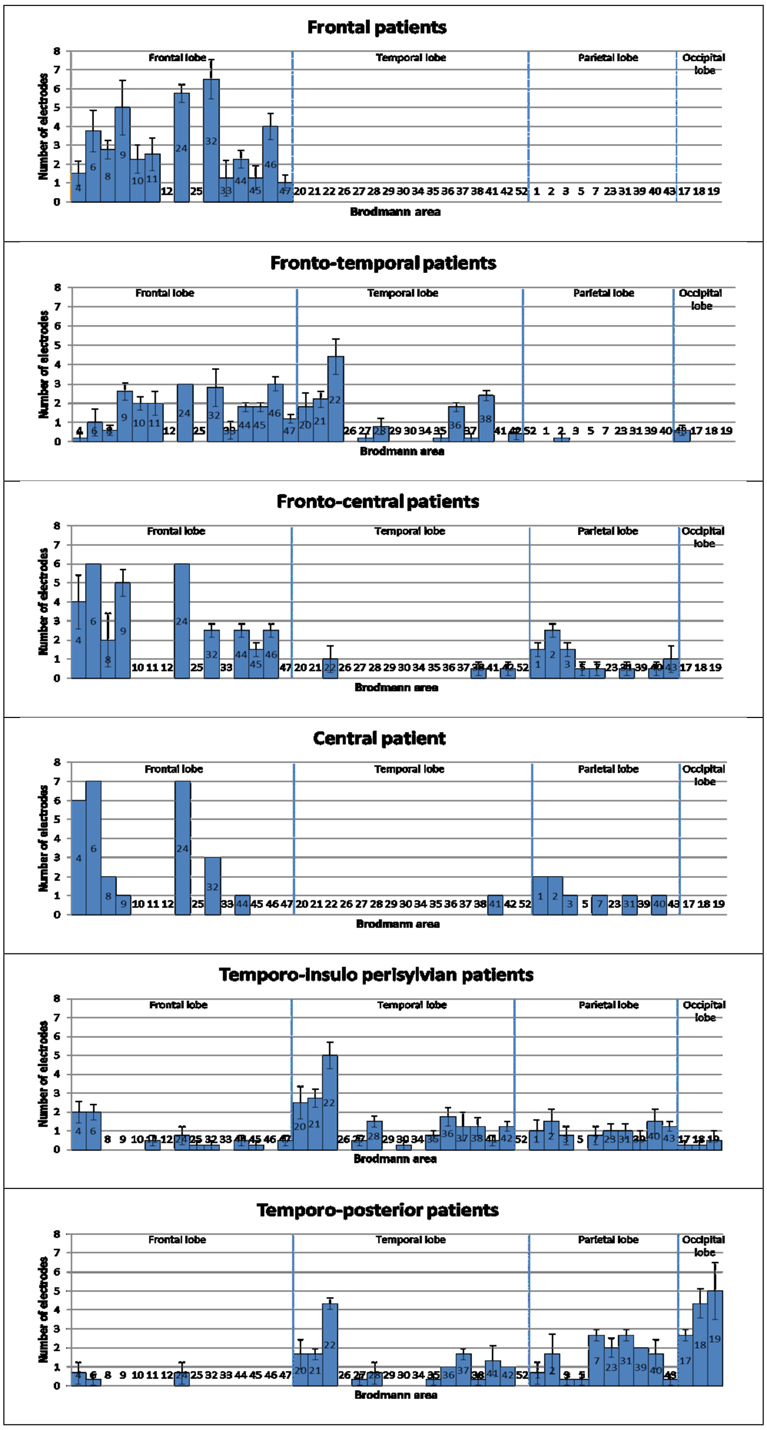

Figure 4.8: Distribution of electrodes in the Brodmann areas according to the exploration pattern. In each histogram the mean and the SD values of the number of electrodes crossing a specific Brodmann area, considering all the patients belonging to the analyzed pattern, are displayed.

Brodmann area	F	FT	FC	C	TIP	TP
	Mean(SD)	Mean(SD)	Mean(SD)		Mean(SD)	Mean(SD)
4	1.5(1.29)	0.2(0.45)	4(2.83)	6	2(1.15)	0.67(1.15)
6	3.75(2.22)	1(1.41)	6(0)	7	2(0.82)	0.33(0.58)
8	2.75(0.96)	0.6(0.55)	2(2.83)	2	0(0)	0(0)
9	5(2.94)	2.6(0.89)	5(1.41)	1	0(0)	0(0)
10	2.25(1.50)	2(0.71)	0(0)	0	0(0)	0(0)
11	2.5(1.73)	2(1.22)	0(0)	0	0.5(0.58)	0(0)
12	0(0)	0(0)	0(0)	0	0(0)	0(0)
24	5.75(0.96)	3(0)	6(0)	7	0.75(0.96)	0.67(1.15)
25	0(0)	0(0)	0(0)	0	0.25(0.50)	0(0)
32	6.5(2.08)	2.8(1.92)	2.5(0.71)	3	0.25(0.50)	0(0)
33	1.25(1.89)	0.6(0.89)	0(0)	0	0(0)	0(0)
44	2.25(0.96)	1.8(0.45)	2.5(0.71)	1	0.5(0.58)	0(0)
45	1.25(1.26)	1.8(0.45)	1.5(0.71)	0	0.25(0.50)	0(0)
46	4(1.41)	3(0.71)	2.5(0.71)	0	0(0)	0(0)
47	1(0.82)	1.2(0.45)	0(0)	0	0.5(0.58)	0(0)
20	0(0)	1.8(1.48)	0(0)	0	2.5(1.73)	1.67(1.53)
21	0(0)	2.2(0.84)	0(0)	0	2.75(0.96)	1.67(0.58)
22	0(0)	4.4(1.82)	1(1.41)	0	5(1.41)	4.33(0.58)
26	0(0)	0(0)	0(0)	0	0(0)	0(0)
27	0(0)	0.2(0.45)	0(0)	0	0.5(0.58)	0.33(0.58)
28	0(0)	0.8(0.84)	0(0)	0	1.5(0.58)	0.67(1.15)
29	0(0)	0(0)	0(0)	0	0(0)	0(0)
30	0(0)	0(0)	0(0)	0	0.25(0.50)	0(0)
34	0(0)	0(0)	0(0)	0	0(0)	0(0)
35	0(0)	0.2(0.45)	0(0)	0	0.75(0.50)	0.33(0.58)
36	0(0)	1.8(0.45)	0(0)	0	1.75(0.96)	1.00(0)
37	0(0)	0.2(0.45)	0(0)	0	1.25(1.50)	1.67(0.58)
38	0(0)	2.4(0.55)	0.5(0.71)	0	1.25(0.96)	0.33(0.58)
41	0(0)	0(0)	0(0)	1	0.5(0.58)	1.33(1.53)
42	0(0)	0.4(0.55)	0.5(0.71)	0	1.25(0.50)	1.00(0)
52	0(0)	0(0)	0(0)	0	0(0)	0(0)
1	0(0)	0(0)	1.5(0.71)	2	1(1.15)	0.67(1.15)
2	0(0)	0.2(0.45)	2.5(0.71)	2	1.5(1.29)	1.67(2.08)
3	0(0)	0(0)	1.5(0.71)	1	0.75(0.96)	0.33(0.58)
5	0(0)	0(0)	0.5(0.71)	0	0(0)	0.33(0.58)
7	0(0)	0(0)	0.5(0.71)	1	0.75(0.96)	2.67(0.58)
23	0(0)	0(0)	0(0)	0	1(0.82)	2.00(1.00)
31	0(0)	0(0)	0.5(0.71)	1	1(0.82)	2.67(0.58)
39	0(0)	0(0)	0(0)	0	0.5(1.00)	2.00(0)
40	0(0)	0(0)	0.5(0.71)	1	1.5(1.29)	1.67(1.53)
43	0(0)	0.6(0.55)	1(1.41)	0	1.25(0.50)	0.33(0.58)
17	0(0)	0(0)	0(0)	0	0.25(0.50)	2.67(0.58)
18	0(0)	0(0)	0(0)	0	0.25(0.50)	4.33(1.53)
19	0(0)	0(0)	0(0)	0	0.5(1.00)	5.00(3.00)

Table 4.5: Mean(SD) of the number of electrodes crossing a Brodmann area considering patients grouped according to their exploration pattern (F: frontal; FT: fronto-temporal; FC: fronto-central; C: central; TIP: temporo-insulo perisylvian; TP: temporo-posterior).

Finally, in Fig. 4.9 it is represented, as a color map, the total number of contacts, considering all the electrodes going through a specific Brodmann area entering inside the cortical surface, that crossed a specific Desikan and Killiany atlas region, divided by the number of electrodes that share this Brodmann area at the entry point. The graphical representations are shown in Fig. 4.10, Fig. 4.11, Fig. 4.12, Fig. 4.13, respectively for the frontal, temporal, parietal and occipital lobes.

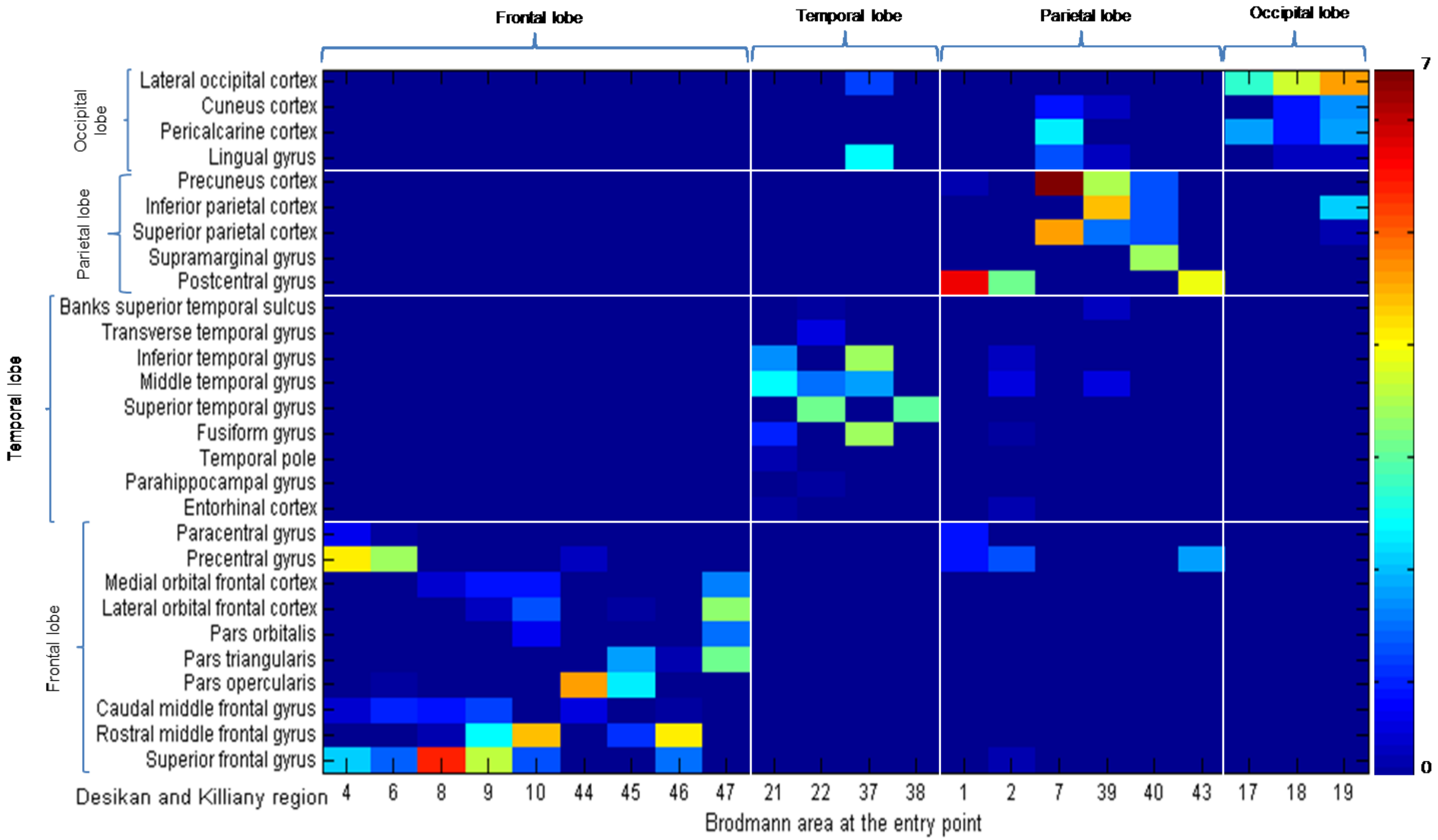

Figure 4.9: Correlation between the Brodmann area at the entry point of the electrodes on the cortical surface and the Desikan and Killiany atlas regions crossed by the contacts.

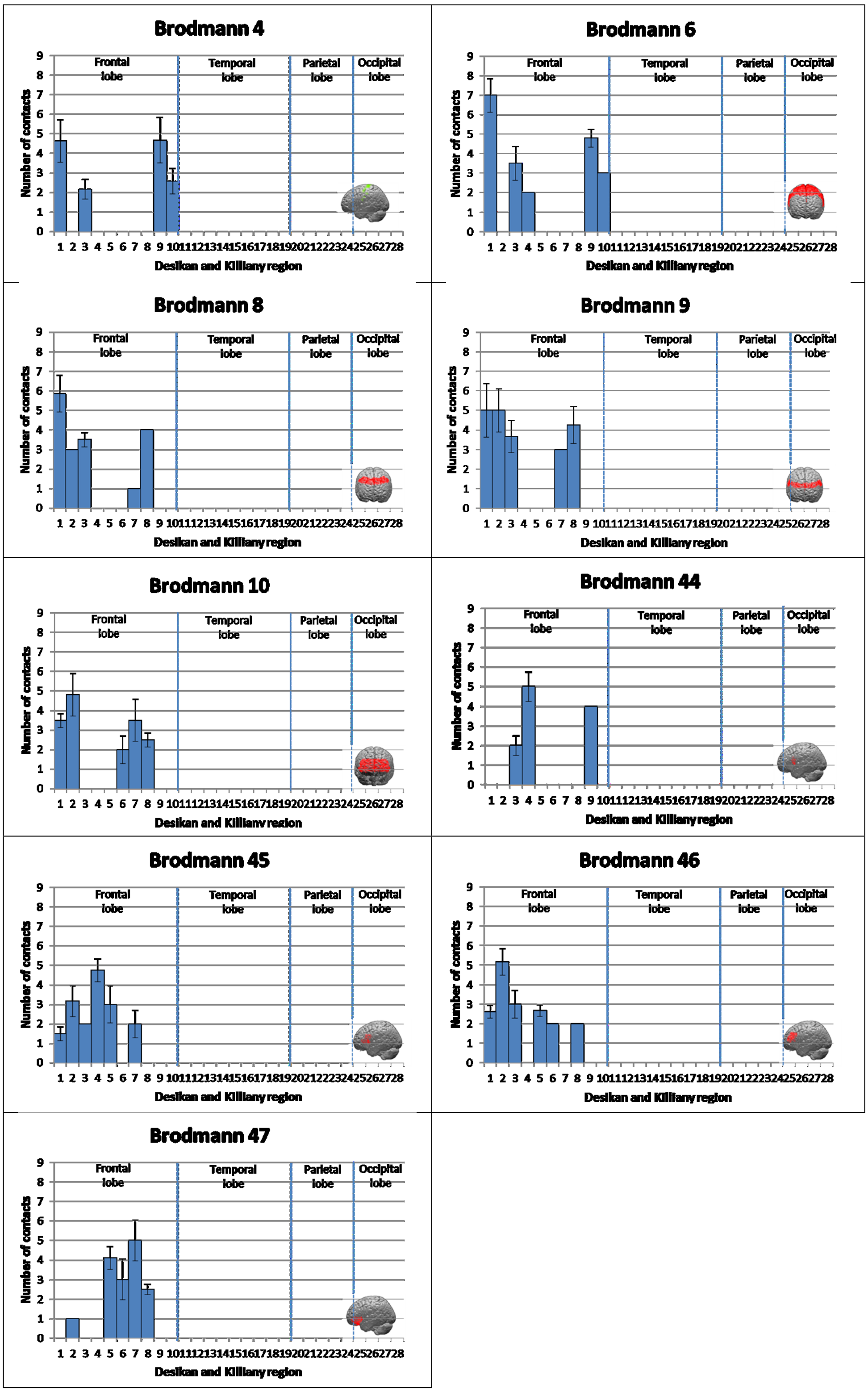

Figure 4.10: Distribution of contacts in the Desikan and Killiany atlas regions according to the Brodmann area crossed by the electrodes at the entry point on the cortical surface. The Brodmann areas located in the frontal lobe are visualized.

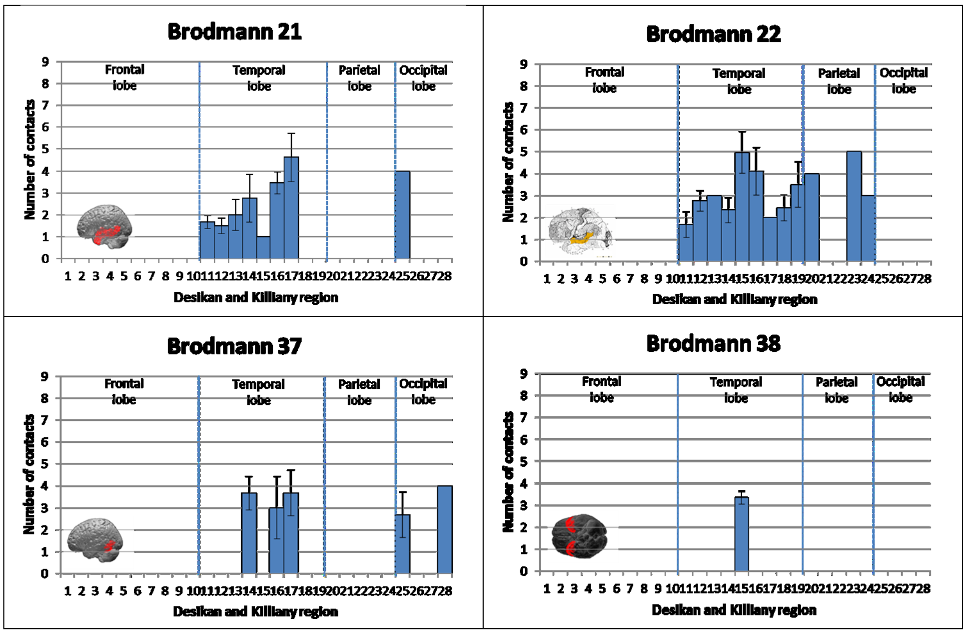

Figure 4.11: Distribution of electrodes contacts in the Desikan and Killiany atlas regions according to the Brodmann area crossed by the electrodes at the entry point on the cortical surface. In each histogram the mean and the standard deviation values of the number of contacts crossing a Desikan and Killiany atlas region, considering all the electrodes crossing a specific Brodmann area as they enter into the pial surface, are displayed. In this figure the Brodmann areas located in the temporal lobe are visualized.

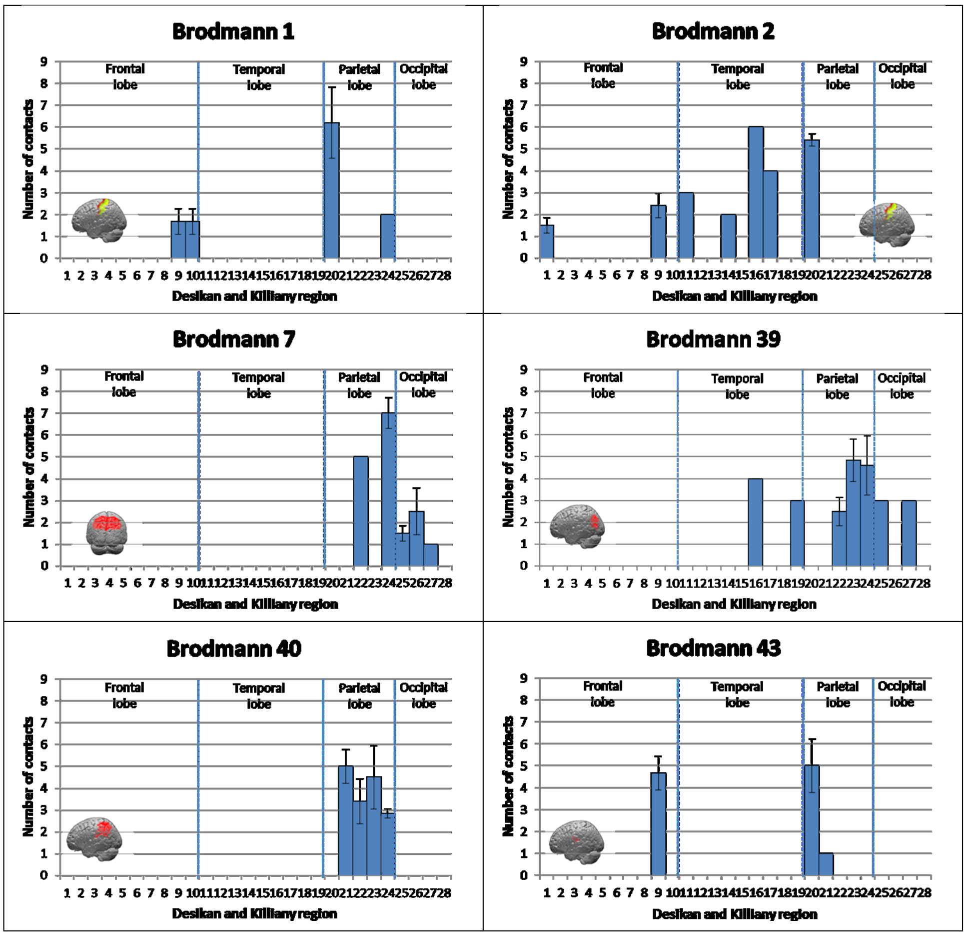

Figure 4.12: Distribution of electrodes contacts in the Desikan and Killiany atlas regions according to the Brodmann area crossed by the electrodes at the entry point on the cortical surface. In each histogram the mean and the standard deviation values of the number of contacts crossing a Desikan and Killiany atlas region, considering all the electrodes crossing a specific Brodmann area as they enter into the pial surface, are displayed. In this figure the Brodmann areas located in the parietal lobe are visualized.

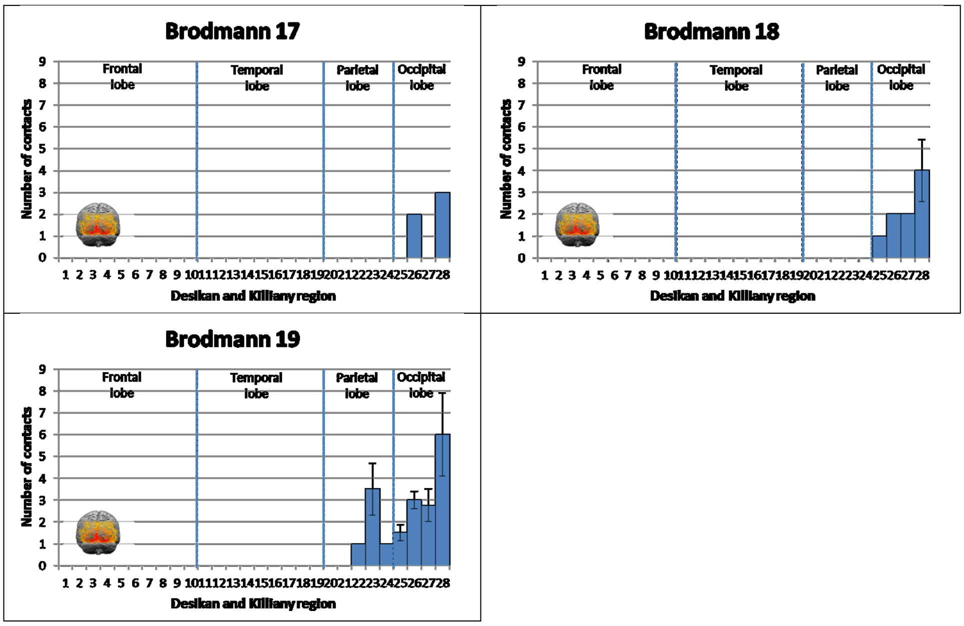

Figure 4.13: Distribution of electrodes contacts in the Desikan and Killiany atlas regions according to the Brodmann area crossed by the electrodes at the entry point on the cortical surface. In each histogram the mean and the standard deviation values of the number of contacts crossing a Desikan and Killiany atlas region, considering all the electrodes crossing a specific Brodmann area as they enter into the pial surface, are displayed. In this figure the Brodmann areas located in the occipital lobe are visualized.

4.4 Electrode curvature analysis

The output of the mixed effects linear regression model is reported in Table 4.6. The electrode intracerebral length is linearly related to the electrode mean curvature with a regression coefficient equal to -0.0002; the estimated regression coefficient for the superior temporal gyrus region (the only region of the Desikan and Killiany atlas resulted correlated with the outcome variable) is 0.0021. The remaining variables (the skull angle and the other atlas regions) are not found to be correlated with the outcome variable.

Variable	Coefficient	SE	P-value
Length	-0.0002	0.00003	<0.0001
Desikan and Killiany atlas region: Superior temporal gyrus	0.0021	0.0008	0.0144

Table 4.6: Output of the mixed effects linear regression model performed on a dataset of 242 electrodes. The skull angle and all other atlas regions were analyzed but not reported because they were not significantly associated with the outcome variable. SE: standard error.

Chapter 5

Discussions and Conclusions

5.1 Discussions and Conclusions

StereoElectroEncephaloGraphy is a diagnostic mini-invasive procedure with the aim to identify the extent of the cortical areas primarily involved in the ictal discharges, i.e. the epileptogenic zone, in patients with partial drug-resistant epilepsy, candidates for the surgical treatment. It consists in the stereotactically implantation of intracerebral multilead electrodes, followed by the video-SEEG monitoring. During this period the electrical activity directly from encephalic structures is recorded and, through electrical stimulation, a cortical functional map is elaborated. Therefore it is important to have accurate mapping tools for localizing the sources of the recorded signal.

The objective of the work is to automatically reconstruct and localize with high accuracy each contact of the implanted electrodes with respect to the structural and functional brain anatomy, thus leading to a correct interpretation of the EEG signal for a correct planning of the subsequent surgical resective procedure. No studies regarding automatic localization of SEEG electrodes contacts have been presented so far, but methods have been developed regarding the localization of subdural grid electrodes and deep brain stimulation electrodes.

The presented method has been integrated in the 3D Slicer software present at the "C. Munari" Centre for Epilepsy and Parkinson Surgery of Niguarda hospital. This work is going to improve the clinical routine at the center: during the monitoring period the epileptologists interpret the SEEG traces having available a 3D Slicer scene containing the acquired patient volumetric imaging and the surface models extracted by FreeSurfer software. The position of each electrode contact is therefore only visually checked. The inputs required for the developed method include both image datasets, which are routinely acquired in the center, and files generated by FreeSurfer and Matlab software. The output is a .csv file, automatically generated for each analyzed patient, containing for every contact of each implanted electrode the information about its position with respect to the gray matter, the Desikan and Killiany atlas and the Brodmann areas. This resulting report allows the creation of a patients database.

Once the input data have been loaded in the Slicer scene, the algorithm takes about 10 seconds for the reconstruction of the selected electrode and its localization (identification of cortical contacts and of the crossed Desikan and Killiany atlas regions and Brodmann areas). In general, considering a mean number of electrodes for patient equal to 13, the time that the method requires to process the entire patient electrodes dataset is about 2/3 minutes. Conversely, the manual definition of each contact on the postoperative CT volume takes about 2 minutes per electrode. Given a mean number of contacts per electrode and per patient respectively equal to 14 and 175, this latter is extremely time consuming for the clinician. The automatism is an advantage of the method.

Electrode curve modelling The third order polynomial is used to model electrode deformation. In fact, an higher degree of the regression curve could modify the real aspect of the electrode. Specifically, on the basis of the surgeon experience (approximately 6.500 electrodes implanted), these have never shown deformations with changes of concavity; once they take a direction, they keep it.

Electrodes identification accuracy The *Automatic electrodes identification* algorithm shows a more accurate behavior than the *Manual electrodes identification* in the localization of electrodes contacts, using as reference the manually identified leads on the postoperative CT volume (Fig. 4.2). The dimension of the voxels of the postoperative volume acquired with the O-arm is 0.4 x 0.4 x 0.8. The resulted median of the Euclidean distances for the *Automatic electrodes identification* (0.529 mm) is comparable with the resolution of the imaging space.

The gold standard, i.e. the manually identified contacts on the postoperative volume, is influenced by the surgeon manual positioning accuracy. For this reason, the surgeon does not consider as qualitatively significant the difference between the two methods, analyzing electrodes non visually deviated, even if quantitatively significant ($p\text{-value}<0.0001$). The difference between the two methods increased (Fig. 4.4 and Table 4.3) when considering a visually deviated electrode with 18 contacts (Fig. 4.3), thus highlighting the ability of the *Automatic electrodes identification* method to model the electrode's trajectory. As reported in the study [14], considering a sample of 1576 electrodes, a percentage of 7.7 bent; since this proportion isn't negligible, for the purpose of electrode reconstruction and contacts localization, the identification of the entry and target points isn't enough. In any case, the *Automatic electrodes identification* algorithm enables the user to select the preferred order of the regression curve to model the electrode trajectory. If the surgeon assumes, by a visual inspection, that the considered electrode hasn't deviated from the original plan, he/she can select the first degree of regression to reconstruct it linearly.

Another benefit is related to vertical implanted electrodes (Fig. 5.1): due to the anisotropic voxel of the O-arm dataset (0.4 x 0.4 x 0.8), contacts of electrodes implanted in the cranio-caudal direction are mainly distributed along the z-axis of the imaging space, whose resolution is half of the one of the other two axes. Contacts artifacts on the postoperative CT volume are then overlapped with each other, leading to hardly distinguishable electrodes leads. In this condition, the visual identification of contacts is difficult and certainly less accurate than their automatic reconstruction and localization.

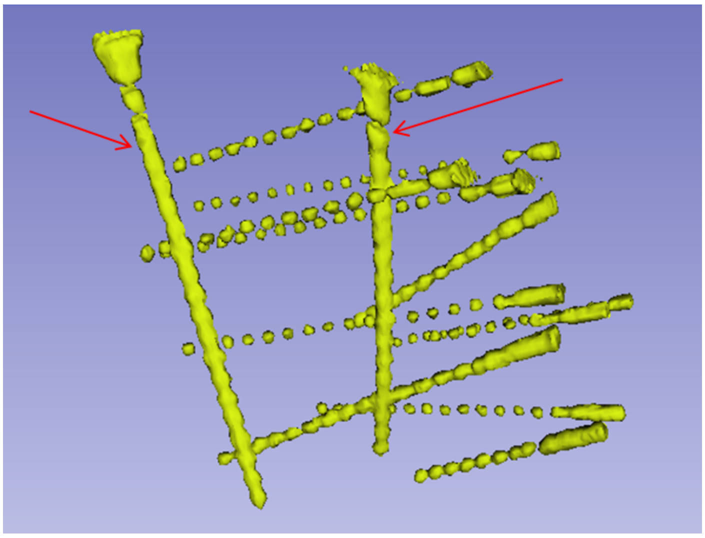

Figure 5.1: Screenshot of the Slicer 3D view displaying electrodes model generated starting from the SEEG skull-stripped volume. Vertical electrodes are indicated with red arrows.

Being the intraoperative photographs, used in [8, 9, 25, 28, 11] to evaluate the localization accuracy, not applicable in the SEEG context, an alternative way, with respect to the gold standard here used, to validate the developed method, may be the usage of a calibrated phantom in which an electrode is fixed.

Electrode exploration analysis Fig. 4.5 shows the distribution of electrodes contacts of the patients grouped according to their patterns with respect to the Desikan and Killiany atlas. Several purely clinical justifications could be done with respect to the numerical values found by the analysis (Fig. 4.6 and Table 4.4). All the electrodes in frontal subjects crossed atlas regions located in the frontal lobe. The region Pars orbitalis (number 6 in Fig. 4.6) is less explored than the others because it is located on the roof of the orbital cavity: implanting an electrode there means an entry point where hair cannot cover the scar, and also the curvature of the bone is unfavorable. The subjects explored with a fronto-temporal pattern have contacts also in the post-central gyrus (number 20 in Fig. 4.6), a region of the parietal lobe; the motivation has to be found in the definition of the exploration pattern, intended as the region explored by most of the electrodes, not all. Considering fronto-central patients, contacts in the Desikan and Killiany atlas regions 15 and 18 (Fig. 4.6) belonging to the temporal lobe are motivated by the interest to reach the insula: whenever the epileptogenic focus is a structure lying on the inferior or mesial surface of the hemisphere, and not on the dorsal or lateral one, structures on the dorsal and lateral surface of the hemisphere must be crossed, even if not interesting. The patient with a central exploration has contacts in regions not located in the central lobe; in fact, considering that one of the purpose of SEEG in the central lobe is to map the motor functions, these contacts in front of and behind the central lobe are used to define, as accurate as possible, the eloquent cortex. For the same reason, also in temporo-posterior subjects there are contacts in central regions, spy for the motor functions.

Similar considerations could be done for the other two analysis (Fig. 4.7 and Fig. 4.9). For example, the Brodmann areas 24 and 35 (Fig. 4.7) are translobar areas, belonging to the frontal, parietal and central lobes; they are crossed by a high number of electrodes in more than one pattern (frontal, fronto-temporal, fronto-central and central). In Fig. 4.9 a pattern in the contacts distribution in the Desikan and Killiany atlas regions, giving the Brodmann area at the electrodes entry point on the cortical surface, can be recognized.

In conclusion, the results of these analysis are congruous with what the surgeon expected, thus highlighting the potentiality of the method to assign to each contact of the implanted electrodes the label of the Desikan and Killiany atlas and the PALS B12 Brodmann atlas, and, in general, to automatically classify the reconstructed contacts with respect to the atlases integrated in Slicer.

Regarding this analysis, two observations must be done. Firstly, in the definition of the exploration patterns, the surgeon distinguishes the central lobe, which is not classify by the classical anatomy. The central lobe is where the primary motor-sensitive cortex is located and it is composed by the following Desikan and Killiany atlas regions: precentral gyrus, paracentral lobule and postcentral gyrus. Secondly, the Desikan and Killiany atlas does not classify the insular lobe even though it is defined by the classical anatomy: its non-classification is a limit of the atlas.

Electrode curvature analysis The multivariate analysis was performed fitting a mixed effects linear regression model. The "patient ID" was considered as random effect and it was included into the model; the other explanatory variables were considered fixed effects. In this way the model is corrected for the dependence of the electrodes implanted in the same patient. There may be, in fact, some factors not included into the model but dependent on the surgical procedure on a specific patient, which can influence the bending.

The first explanatory variable significantly associated to the mean curvature is the electrode intracerebral length. The negative regression coefficient associated to the intracerebral length can be explained by considering that the majority of the electrodes included in the modeled dataset were not visually deviated. In fact, with respect to the total of 242 electrodes, only one is visually deviated: this electrode has a MCI equal to 0.01, an order of magnitude higher than the median curvature of the entire dataset, and a intracerebral length equal to 90.459 mm, i.e. twice the median value of the considered dataset (Table 3.2). All other electrodes are not visually deviated; thus, the only deviated electrode has no effect on the whole dataset. Given that the negative (-0.0002) relation found between the electrode curvature and the intracerebral length is logically unacceptable, it will be necessary to perform the analysis on a dataset including a greater number of visually deviated electrodes.

The second explanatory variable significantly associated to the mean curvature is the superior temporal gyrus (Desikan and Killiany atlas region). The significant relation between the electrode curvature and the passage through the superior temporal gyrus is explained considering that those electrodes have to cross more arachnoid than others in order to reach the insula. Stretching several arachnoid layers and to pierced them, results in a bending of the electrode.

5.2 Future work

The developed method shows good capacities to reconstruct and localize with high accuracy multilead intracerebral electrodes. Several possible developments might be considered.

- The integration in the module of the automatic centroids identification, first step of the *Automatic electrodes identification* algorithm. At the moment this analysis must be performed before using the module in order to obtain its output file that constitutes the input of the following step of the *Automatic electrodes identification* algorithm.

- The automatic detection of the electrode deviation through the definition of some parameters, for example the electrode's curvature, with respect to which it may be possible to classify an electrode as deviated or not. Based on the result of this test, the user can model the reconstructed electrode with a straight line, if it hasn't deviated, or choose higher degree of regression if the electrode has deviated.

- Enlarging the method's localization capability through the integration of other atlases that have not been considered yet. While the Desikan and Killiany atlas was already integrated in Slicer, the PALS B12 Brodmann atlas has been integrated during this work using the segmentation of the cortex and the lookup table given by the FreeSurfer software.

- The association of each reconstructed and localized electrode contact with the recorded electrical signal. The tool thus developed might facilitate the correlation between the signal and the crossed cortical regions and eloquent cortex, helping the planning of the resective surgery.

- The creation of an electrophysiological atlas according to the Brodmann areas, i.e. a spatial map of electrophysiological information, such the electrical signal recorded by the implanted electrodes and the Brodmann areas crossed by each of them (module output), acquired for a high number of patients who underwent SEEG at the center. Starting from, for each subject, the parcellation of the cerebral cortex based on the Brodmann areas and the correspondence between the Brodmann areas crossed by an electrode and the signal recorded by this latter, a cortical atlas may be generated through a registration procedure.

Bibliography

[1] R. Mai and F. Cardinale, "Robotic implantation of intracerebral electrodes in epilepsy surgery," *Congress quarterly*, pp. 24–26, 2011.

[2] C. Pollo, F. Vingerhoets, E. Pralong, J. Ghika, P. Maeder, R. Meuli, J. Thiran, and J. Villemure, "Localization of electrodes in the subthalamic nucleus on magnetic resonance imaging," *Journal of neurosurgery*, vol. 106, no. 1, pp. 36–44, 2007.

[3] F. Vergani, A. Landi, A. Antonini, M. Parolin, R. Cilia, M. Grimaldi, C. Ferrarese, S. Gaini, and E. Sganzerla, "Anatomical identification of active contacts in subthalamic deep brain stimulation," *Surgical neurology*, vol. 67, no. 2, pp. 140–146, 2007.

[4] C. Butson, S. Cooper, J. Henderson, and C. McIntyre, "Patient-specific analysis of the volume of tissue activated during deep brain stimulation," *Neuroimage*, vol. 34, no. 2, pp. 661–670, 2007.

[5] S. Pinto, J. Le Bas, L. Castana, P. Krack, P. Pollak, and A. Benabid, "Comparison of two techniques to postoperatively localize the electrode contacts used for subthalamic nucleus stimulation," *Neurosurgery*, vol. 60, no. 4, p. 285, 2007.

[6] S. Hemm, J. Coste, J. Gabrillargues, L. Ouchchane, L. Sarry, F. Caire, F. Vassal, C. Nuti, P. Derost, F. Durif, *et al.*, "Contact position analysis of deep brain stimulation electrodes on post-operative ct images," *Acta neurochirurgica*, vol. 151, no. 7, pp. 823–829, 2009.

[7] D. Kovalev, J. Spreer, J. Honegger, J. Zentner, A. Schulze-Bonhage, and H. Huppertz, "Rapid and fully automated visualization of subdural electrodes in the presurgical evaluation of epilepsy patients," *American journal of neuroradiology*, vol. 26, no. 5, pp. 1078–1083, 2005.

[8] A. I. Yang, X. Wang, W. Doyle, E. Halgren, C. Carlson, T. L. Belcher, S. S. Cash, O. Devinsky, and T. Thesen, "Localization of dense intracranial electrode arrays using magnetic resonance imaging," *Neuroimage*, 2012.

[9] A. Dykstra, A. Chan, B. Quinn, R. Zepeda, C. Keller, J. Cormier, J. Madsen, E. Eskandar, and S. Cash, "Individualized localization and cortical surface-based registration of intracranial electrodes," *NeuroImage*, 2011.

[10] S. Wagner, J. Kuß, T. Meyer, M. Kirsch, and U. Morgenstern, "An integrated tool for automated visualization of subdural electrodes in epilepsy surgery evaluation," *International journal of computer assisted radiology and surgery*, vol. 4, no. 6, pp. 609–616, 2009.

[11] S. S. Dalal, E. Edwards, H. E. Kirsch, N. M. Barbaro, R. T. Knight, and S. S. Nagarajan, "Localization of neurosurgically implanted electrodes via photograph–mri–radiograph coregistration," *Journal of neuroscience methods*, vol. 174, no. 1, pp. 106–115, 2008.

[12] P. Kahane, E. Landré, L. Minotti, S. Francione, and P. Ryvlin, "The bancaud and talairach view on the epileptogenic zone: a working hypothesis," *Epileptic disorders*, vol. 8, pp. 16–26, 2006.

[13] J. Talairach, *Approche nouvelle de la neurochirurgie de l'épilepsie: methodologie stéréotaxique et resultats thérapeutiques: XXIV congrès annuel; Marseille, 25-28 Juin 1974.* Masson, 1974.

[14] F. Cardinale, M. Cossu, L. Castana, G. Casaceli, M. Schiariti, A. Miserocchi, D. Fuschillo, A. Moscato, C. Caborni, G. Arnulfo, *et al.*, "Stereoelectroencephalography: Surgical methodology, safety and stereotactic application accuracy in five hundred procedures," *Neurosurgery*, 2012.

[15] J. Gonzalez-Martinez, J. Bulacio, A. Alexopoulos, L. Jehi, W. Bingaman, and I. Najm, "Stereoelectroencephalography in the difficult to localize refractory focal epilepsy: Early experience from a north american epilepsy center," *Epilepsia*, 2012.

[16] C. Munari, D. Hoffmann, S. Fracione, P. Kahane, L. Tassi, G. Russo, and A. Benabid, "Stereo-electroencephalography methodology: advantages and limits," *Acta Neurologica Scandinavica*, vol. 89, no. S152, pp. 56–67, 2009.

[17] F. Ozlen, Z. Asan, T. Tanriverdi, A. Kafadar, C. Ozkara, E. Ozyurt, and M. Uzan, "Surgical morbidity of invasive monitoring in epilepsy surgery: an experience from a single institution," *Turk Neurosurg*, vol. 20, no. 3, pp. 364–372, 2010.

[18] M. Guenot, J. Isnard, P. Ryvlin, C. Fischer, K. Ostrowsky, F. Mauguiere, and M. Sindou, "Neurophysiological monitoring for epilepsy surgery: the talairach seeg method," *Stereotactic and functional neurosurgery*, vol. 77, no. 1-4, pp. 29–32, 2001.

[19] T. Tanriverdi, A. Ajlan, N. Poulin, and A. Olivier, "Morbidity in epilepsy surgery: an experience based on 2449 epilepsy surgery procedures from a single institution," *Journal of neurosurgery*, vol. 110, no. 6, pp. 1111–1123, 2009.

[20] S. Ferrand-Sorbets, M. Delphine Taussig, M. Fohlen, C. Bulteau, G. Dorfmuller, and O. Delalande, "Frameless stereotactic robot-guided placement of depth electrodes for stereo-electroencephalography in the presurgical evaluation of children with drug-resistant focal epilepsy," in *CNS Annual Meeting*, 2010.

[21] F. Chassoux, B. Devaux, E. Landré, B. Turak, F. Nataf, P. Varlet, J. Chodkiewicz, and C. Daumas-Duport, "Stereoelectroencephalography in focal cortical dysplasia a 3d approach to delineating the dysplastic cortex," *Brain*, vol. 123, no. 8, pp. 1733–1751, 2000.

[22] J. Saint-Cyr, T. Hoque, L. Pereira, J. Dostrovsky, W. Hutchison, D. Mikulis, A. Abosch, E. Sime, A. Lang, and A. Lozano, "Localization of clinically effective stimulating electrodes in the human subthalamic nucleus on magnetic resonance imaging," *Journal of neurosurgery*, vol. 97, no. 5, pp. 1152–1166, 2002.

[23] P. Starr, C. Christine, P. Theodosopoulos, N. Lindsey, D. Byrd, A. Mosley, and W. Marks Jr, "Implantation of deep brain stimulators into subthalmic nucleus: technical approach and magnetic imaging-verified electrode locations," *Journal of neurosurgery*, vol. 97, no. 2, pp. 370–387, 2002.

[24] H. Andreas, H. Huppertz, R. Comeau, J. Honegger, J. Spreer, and J. Zentner, "Visualization of subdural strip and grid electrodes using curvilinear reformatting of 3d mr imaging data sets," *American journal of neuroradiology*, vol. 23, no. 3, pp. 400–403, 2002.

[25] F. Sebastiano, G. Di Gennaro, V. Esposito, A. Picardi, R. Morace, A. Sparano, A. Mascia, C. Colonnese, G. Cantore, and P. Quarato, "A rapid and reliable procedure to localize subdural electrodes in presurgical evaluation of patients with drug-resistant focal epilepsy," *Clinical neurophysiology*, vol. 117, no. 2, pp. 341–347, 2006.

[26] P. Winkler, C. Vollmar, K. Krishnan, T. Pfluger, H. Brückmann, and S. Noachtar, "Usefulness of 3-d reconstructed images of the human cerebral cortex for localization of subdural electrodes in epilepsy surgery," *Epilepsy research*, vol. 41, no. 2, pp. 169–178, 2000.

[27] A. Immonen, L. Jutila, M. Könönen, E. Mervaala, J. Partanen, M. Puranen, J. Rinne, A. Ylinen, and M. Vapalahti, "3-d reconstructed magnetic resonance imaging in localization of subdural eeg electrodes: Case illustration," *Epilepsy research*, vol. 54, no. 1, pp. 59–62, 2003.

[28] D. Hermes, K. Miller, H. Noordmans, M. Vansteensel, and N. Ramsey, "Automated electrocorticographic electrode localization on individually rendered brain surfaces," *Journal of neuroscience methods*, vol. 185, no. 2, pp. 293–298, 2010.

[29] S. M. Smith, "Fast robust automated brain extraction," *Human brain mapping*, vol. 17, no. 3, pp. 143–155, 2002.

[30] R. Desikan, F. Ségonne, B. Fischl, B. Quinn, B. Dickerson, D. Blacker, R. Buckner, A. Dale, R. Maguire, B. Hyman, *et al.*, "An automated labeling system for subdividing the human cerebral cortex on mri scans into gyral based regions of interest," *Neuroimage*, vol. 31, no. 3, pp. 968–980, 2006.

[31] D. Van Essen *et al.*, "A population-average, landmark-and surface-based (pals) atlas of human cerebral cortex," *Neuroimage*, vol. 28, no. 3, pp. 635–662, 2005.

[32] A. Gray, E. Abbena, and S. Salamon, *Modern differential geometry of curves and surfaces with Mathematica.* Chapman & Hall, 2006.